MCB
Journals.ASM.org

C11orf83, a Mitochondrial Cardiolipin-Binding Protein Involved in bc_1 Complex Assembly and Supercomplex Stabilization

Marjorie Desmurs,[a] Michelangelo Foti,[b] Etienne Raemy,[c] Frédéric Maxime Vaz,[d] Jean-Claude Martinou,[c] Amos Bairoch,[a,e] Lydie Lane[a,e]

Department of Human Protein Sciences, University of Geneva, Geneva, Switzerland[a]; Department of Cell Physiology and Metabolism, University of Geneva, Geneva, Switzerland[b]; Department of Cell Biology, University of Geneva, Geneva, Switzerland[c]; Laboratory Genetic Metabolic Diseases, Department of Clinical Chemistry and Pediatrics, University of Amsterdam, Academic Medical Center, Amsterdam, The Netherlands[d]; CALIPHO Group, SIB Swiss Institute of Bioinformatics, Geneva, Switzerland[e]

Mammalian mitochondria may contain up to 1,500 different proteins, and many of them have neither been confidently identified nor characterized. In this study, we demonstrated that C11orf83, which was lacking experimental characterization, is a mitochondrial inner membrane protein facing the intermembrane space. This protein is specifically associated with the bc_1 complex of the electron transport chain and involved in the early stages of its assembly by stabilizing the bc_1 core complex. C11orf83 displays some overlapping functions with Cbp4p, a yeast bc_1 complex assembly factor. Therefore, we suggest that C11orf83, now called UQCC3, is the functional human equivalent of Cbp4p. In addition, C11orf83 depletion in HeLa cells caused abnormal crista morphology, higher sensitivity to apoptosis, a decreased ATP level due to impaired respiration and subtle, but significant, changes in cardiolipin composition. We showed that C11orf83 binds to cardiolipin by its α-helices 2 and 3 and is involved in the stabilization of bc_1 complex-containing supercomplexes, especially the III_2/IV supercomplex. We also demonstrated that the OMA1 metalloprotease cleaves C11orf83 in response to mitochondrial depolarization, suggesting a role in the selection of cells with damaged mitochondria for their subsequent elimination by apoptosis, as previously described for OPA1.

Mitochondria are membrane-enclosed organelles composed of several compartments which perform specialized and interconnected functions such as oxidative phosphorylation (OXPHOS), cell death, or carbohydrate and fatty acid metabolisms. OXPHOS, which provides most of the ATP used by the cell, takes place in the inner membrane (IM) and involves five complexes. Redox reactions are carried out by complex I (NADH: ubiquinone oxidoreductase; EC 1.6.5.3), complex II (succinate: ubiquinone oxidoreductase; EC 1.3.5.1), complex III (ubiquinol: ferricytochrome *c* oxidoreductase; EC 1.10.2.2), and complex IV (cytochrome *c* oxidoreductase; EC 1.9.3.1). Then, the ATP synthase, complex V (F_1F_0 ATPase; EC 3.6.3.14), uses the energy released by respiration for ATP generation. The assembly of the OXPHOS complexes requires additional nuclear proteins called assembly factors (1). The physiological importance of these assembly factors is proven by the number of human diseases associated with mutations in genes encoding them (1).

Complex III, also called cytochrome bc_1 complex, is a central component of the electron transport chain (ETC). It transfers electrons from coenzyme Q reduced either by complex I through NADH-linked substrates or by complex II through reduced flavin adenine dinucleotide ($FADH_2$)-linked substrates to cytochrome *c*. The mammalian bc_1 complex, which forms as a stable dimer (2), is composed of 11 subunits, among which only MT-CYB is encoded by the mitochondrial genome (3, 4). Most of the work on the bc_1 complex assembly has been performed with *Saccharomyces cerevisiae* and has shown this to be a multistep process involving several subcomplexes and assembly factors (5, 6). Despite the presence of an additional subunit in the mammalian bc_1 complex, corresponding to the cleaved presequence of UQCRFS1, the structures of the bc_1 complex in yeast and mammals are similar (3, 7). Whereas 13 bc_1 complex assembly factors were identified in yeast, only 5 are currently characterized in mammals: BCS1L (8), TTC19 (9), UQCC1 and UQCC2 (10), and LYRM7 (11). Deleterious mutations in the *BCS1L* (12) and *TTC19* (9) genes were reported to cause GRACILE (growth retardation, amino aciduria, cholestasis, iron overload, lactic acidosis, and early death) syndrome and neurological impairments, respectively, due to a defective bc_1 complex assembly.

In the IM, the dimeric bc_1 complex (III_2) can associate with complex I and/or complex IV to form supercomplexes (SC) (13). The functional role of these SC is still under debate, but recent studies have proposed that they can participate in electron transfer and substrate channeling (14), reduce oxidative damage by decreasing the generation of reactive oxygen species by complex I (15), and confer structural stability on respiratory enzymes (16, 17). Three SC-stabilizing factors were recently identified, COX7A2L in mammals (18, 19) and Rcf1p and Rcf2p in yeast (20, 21), which are orthologs of HIGD1A and HIGD2A, respectively.

In mammals, mitochondria may contain up to 1,500 different proteins (22, 23). About 900 of them have been identified and characterized, but the others lack experimental validation (24, 25). We can speculate that several assembly or stabilizing factors of

Received 13 August 2014 **Returned for modification** 13 October 2014
Accepted 7 January 2015

Accepted manuscript posted online 20 January 2015

Citation Desmurs M, Foti M, Raemy E, Vaz FM, Martinou J-C, Bairoch A, Lane L. 2015. C11orf83, a mitochondrial cardiolipin-binding protein involved in bc_1 complex assembly and supercomplex stabilization. Mol Cell Biol 35:1139–1156. doi:10.1128/MCB.01047-14.

Address correspondence to Marjorie Desmurs, marjorie.desmurs@unige.ch, or Lydie Lane, lydie.lane@isb-sib.ch.

Supplemental material for this article may be found at http://dx.doi.org/10.1128/MCB.01047-14.

doi:10.1128/MCB.01047-14

OXPHOS complexes and SC are still unidentified. In this study, we determined that C11orf83 is a mitochondrial protein, targeted and anchored in the IM by its N-terminal section. We showed that C11orf83 can bind to the mitochondrial phospholipids cardiolipin (CL) and phosphatidic acid (PA) independently of this N-terminal membrane-anchoring region. C11orf83-deficient cells displayed abnormal mitochondria with an impaired OXPHOS due to a bc_1 complex assembly deficiency at early stages and to a decrease of the amounts of SC, especially the III_2/IV SC. Moreover, we showed that C11orf83 is a target of OMA1, a mitochondrial metalloprotease, upon mitochondrial depolarization. Taken together, our results demonstrate that C11orf83 is a new assembly factor of the bc_1 complex and also a stabilizing factor of the III_2/IV SC and thus is required for proper mitochondrial morphology and function.

MATERIALS AND METHODS

Reagents and antibodies. Nigericin, E-64-D, carbonyl cyanide *p*-trifluoromethoxyphenylhydrazone (FCCP), oligomycin A, actinomycin D, valinomycin, pepstatin A, and z-VAD-FMK were from Enzo Life Sciences (Lausen, Switzerland). Digitonin was from EMD Millipore (Darmstadt, Germany). Proteinase K was provided by Macherey-Nagel (Düren, Germany). Saponin, *n*-dodecyl-β-D-maltoside (DDM), carbonyl cyanide *m*-chlorophenylhydrazone (CCCP), isopropyl-β-D-thiogalactoside (IPTG), glutathione, glutathione-Sepharose beads, rotenone, dimethyl sulfoxide (DMSO), *N*-tosyl-L-phenylalanine chloromethyl ketone (TPCK), phenylmethanesulfonyl fluoride (PMSF), 3,4-dichloroisocoumarin (DCI), 1,10-phenanthroline (O-PHE), decylubiquinol, cytochrome *c*, 2,6-dicholorophenolindophenol sodium salts (DCPIP), succinic acid, potassium cyanide (KCN), oxaloacetic acid, 5-5′-dithiobis(2-nitrobenzoic acid) (DTNB), malonic acid, ubiquinone, lactate dehydrogenase, pyruvate kinase, phosphoenolpyruvate, and antimycin A were from Sigma-Aldrich (St. Louis, MO).

Mouse polyclonal anti-C11orf83 polyclonal antibody (PAb) was from Primm srl (Milan, Italy). Mouse monoclonal anti-OPA1 antibody (612606) was from BD Biosciences (NJ). Sheep polyclonal anti-cytochrome *c* antibody (ab49879) was from Abcam (Cambridge, United Kingdom). Rabbit polyclonal antibodies obtained from commercial sources were anti-FIS1 (sc-98900) and anti-SIRT3 (sc-99143) from Santa Cruz Biotechnology (Santa Cruz, CA), anti-COX4 from Cell Signaling Technology (Danvers, MA), anti-OMA1 (NBP1-56970) from Novus Biological (Littleton, CO), anti-β-catenin (C2206) from Sigma-Aldrich, and anti-DIABLO (ADI-905-244) from Enzo Life Sciences. All the other rabbit polyclonal antibodies were kindly provided by the Human Protein Atlas team (26): anti-ATP5B (HPA001520), anti-C11orf83 (HPA046851), anti-CYC1 (HPA001247), anti-glyceraldehyde-3-phosphate dehydrogenase (anti-GAPDH) (HPA040067), anti-NDUFB6 (HPA044001), anti-NDUFV2 (HPA003404), anti-SDHB (HPA002868), anti-TIMM44 (HPA043052), anti-UQCRB (HPA043060), anti-UQCRC1 (HPA002815), anti-UQCRFS1 (HPA041863), and anti-UQCRQ (HPA046693). The mouse antibodies against tags were polyclonal anti-V5 (MCA2892GA; Abd Serotec, Raleigh, NC), monoclonal anti-glutathione *S*-transferase (anti-GST) (ab92; Abcam), and monoclonal anti-green fluorescent protein (anti-GFP) (11814460001; Roche Applied Science, Penzberg, Germany). Secondary antibodies for Western blotting were rabbit anti-sheep IgG (sc-2770; Santa Cruz Biotechnology) and goat anti-mouse and anti-rabbit IgG coupled to horseradish peroxidase (62-6520 and G-21234, respectively; Life Technologies, Carlsbad, CA). For immunofluorescence, secondary antibodies were goat anti-mouse antibody conjugated with Alexa 488 and anti-rabbit antibody conjugated with rhodamine (Life Technologies).

Cell lines, DNA transfection, and siRNA transfection. HeLa cells were maintained at 37°C with 5% CO_2–95% air in Dulbecco's modified Eagle medium (DMEM), low glucose (Life Technologies), supplemented with 10% fetal bovine serum (Life Technologies). HeLa cell lines stably downregulating C11orf83 (sh-1 and sh-2) and sh control (sh CTL) cell lines were established as described previously (27). DNA transfection was performed with X-tremeGENE transfection reagent (Roche Applied Science) according to the manufacturer's instructions. All the small interfering RNA (siRNA) transfections were performed with Lipofectamine RNAiMAX transfection reagent (Life Technologies) according to the manufacturer's instructions.

cDNA cloning, plasmid construction, site-directed point mutagenesis, shRNA sequence, and siRNA. The following primers were used to amplify a 279-bp DNA fragment containing the C11orf83 coding region from cDNA of HeLa cells: 5′-CACCATGGATTCCTTGCGGAAAATGCTGATCTC-3′ and 5′-CGGTGACCTCCCGCCGGCG-3′. The fragment was cloned into pENTR/SD/D-TOPO (Life Technologies) and recombined into the Gateway pcDNA3.2-DEST vector (Life Technologies) for the expression of C11orf83-V5 fusion protein. An 88-bp DNA fragment containing the coding sequence for the first 23 amino acids (aa) of C11orf83 was amplified from pcDNA3.2-C11orf83-V5 using 5′-CACCATGGATTCCTTGCGGAAAATGCTGATCTC-3′ and 5′-CGCGTAGCCCACGCCAGCCC-3′ as primers. After being cloned into pENTR/SD/D-TOPO, this fragment was recombined into the Gateway pcDNA-DEST47 vector (Life Technologies), allowing the expression of WT-N23-GFP fusion protein. Mutated plasmids were obtained by the QuikChange site-directed mutagenesis kit (Agilent Technologies, Santa Clara, CA). The following primers were used for mutagenesis experiments: R5AK6A (5′-CAGTCGCAATGGCGGCCGCAGGGGCTGGCG-3′) and R5DK6D (5′-CCAGCATTGCGACTGAGATCAGCATGTCGTCCAAGGAATCCATGG-3′). For GST fusion constructs, the primers used to amplify the C11orf83 full-length cDNA and the cDNA of C11orf83 depleted of its N-terminal transmembrane domain (Δ23C11orf83) were either 5′-CACCGATTCCTTGCGGAAAATGCTGATCTCAGT-3′ or 5′-CACCCTCCTCGTTATCGTGACCCCGG-3′, respectively, and 5′-TCACGGTGACCTCCCGCCG-3′. 5′-CACCCTGCAGGACCCAAGGAGCAGGGAG-3′ and 5′-TTATCACCAGTTCTTCCTCCAGGCCACGTTC-3′ were used to amplify helix 3 sequence from the full-length C11orf83 cDNA. The DNA fragment of C11orf83 helix 2 was obtained by annealing 5′-CACCCTCCTCGTTATCGTGACCCCGGGAGAGCGGCGGAAGCAGGAAATGCTAAAGGAGATGCCATAATGA-3′ and 5′-TCATTATGGCATCTCCTTTAGCATTTCCTGCTTCCGCCGCTCTCCCGGGGTCACGATAACGAGGAGGGTG-3′. All these fragments were then cloned into pENTR/D-TOPO (Life Technologies) and recombined into the Gateway pDEST15 vector (Life Technologies). The recombinant GST-helix 2-helix 3 protein was obtained by site-directed mutagenesis on the pDEST15 GST-Δ23C11orf83 plasmid using the following primers: 5′-CTGGAGGAAGAACTGGTAGTAAGGCGGCGAAGGCGGCG-3′ and 5′-CGCCGCCTTCGCCGCCTTACTACCAGTTCTTCCTCCAG-3′. The following sequence corresponds to the shRNA used to establish HeLa cell lines downregulating C11orf83: AAAACGGATGTGGTGAACTGAAATTGGATCCAATTTCAGTTCACCACATCCG. OMA1 expression was downregulated by 25 pmol of siRNA (s41775; Life Technologies). As a control siRNA, the silencer select negative control 1 was used at 25 pmol (4390843; Life Technologies).

Imaging. HeLa cells were grown on coverslips and fixed with cold acetone for 5 min at room temperature (RT) (for anti-C11orf83 antibody only) or with 4% paraformaldehyde for 15 min at RT (for all other antibodies). After three washes in phosphate-buffered saline (PBS), cells were permeabilized and blocked with 0.25% Triton X-100 and 5% bovine serum albumin (BSA) in PBS for 1 h at RT. After blocking, cells were incubated for 2 h at RT with mouse polyclonal anti-C11orf83 (1/100) or mouse monoclonal anti-V5 (1/400) and rabbit monoclonal anti-COX4 (1/400) in PBS containing 5% BSA and 0.25% Triton X-100. After three washes in PBS containing 5% BSA and 0.25% Triton X-100, cells were incubated with secondary antibodies (1/400) for 1 h at RT. The slides were mounted with Mowiol medium containing diamidino-2-phenylindole (DAPI). Images were acquired using a confocal microscope with a 63× oil objective (LSM 700; Carl Zeiss, Oberkochen, Germany) and analyzed by Zen software (Carl Zeiss).

Preparation of the mitochondrion-enriched fraction and Na_2CO_3 and proteinase K assays. HeLa cells were collected in ice-cold mitochondrial buffer (MB; 210 mM mannitol, 70 mM sucrose, 10 mM HEPES, 1 mM EDTA [pH 7.5]) with protease inhibitor cocktail (Roche Applied Science). Cells were placed in a precooled glass Potter-Elvehjem homogenizer and were broken by 150 strokes using a motor-driven tightly fitting glass/Teflon Potter-Elvehjem homogenizer. Homogenates were centrifuged at 600 × *g* for 10 min at 4°C. The resulting supernatant was further centrifuged at 7,000 × *g* for 10 min at 4°C. The obtained pellet was washed with ice-cold MB, transferred to a 1.5-ml microcentrifuge tube, and centrifuged at 7,000 × *g* for 10 min at 4°C. This washed pellet containing mitochondria was resuspended in MB. The protein concentration of this mitochondrion-enriched fraction was determined using the Bradford method. For the separation of membrane from soluble proteins, 100 μg of proteins from the mitochondrion-enriched fraction were treated with 0.1 M sodium carbonate (pH 11) for 20 min on ice. After treatment, the suspension was centrifuged at 100,000 × *g* for 30 min at 4°C. The pellet (membrane fraction) was resuspended in 50 μl of SDS-PAGE loading buffer. The supernatant (soluble proteins) was collected, precipitated using trichloroacetic acid, and resuspended in 50 μl of SDS-PAGE loading buffer. An equal volume of each sample was loaded and run on a 12% SDS-PAGE gel. After transfer to a polyvinylidene difluoride (PVDF) membrane (GE Healthcare, Buckinghamshire, United Kingdom), an immunoblotting analysis was performed. For proteinase K protection assays, 100 μg of proteins from the mitochondrion-enriched fraction was preincubated with or without 0.5% saponin for 30 min at 4°C before addition of 20 μg of proteinase K to obtain a final concentration of 0.25% saponin. In a negative-control tube, 5 mM PMSF was added at the same time as proteinase K. After 30 min of RT incubation, proteinase K digestion was stopped with 5 mM PMSF. After loading buffer addition, an equal volume of each sample was loaded and run in a 12% SDS-PAGE gel. Western blot analysis was performed following protein transfer to a PVDF membrane.

Isolation of mitochondria from the mitochondrion-enriched fraction. The mitochondrion-enriched pellet was resuspended in 1 ml of isolation buffer (10 mM Tris-morpholinepropanesulfonic acid [MOPS], 1 mM EGTA–Tris, 250 mM sucrose [pH 7.4]) and added on top of a discontinuous sucrose gradient consisting of 19 ml of 1.2 M sucrose, 1 mM EDTA, and 0.1% BSA in 10 mM HEPES (pH 7.4) over 16 ml of 1.6 M sucrose, 1 mM EDTA, and 0.1% BSA in 10 mM HEPES (pH 7.4). Samples were placed in a Beckman SW28 rotor and centrifuged at 82,700 × *g* for 2 h 20 min at 4°C. Mitochondria were recovered at the 1.6 M/1.2 M sucrose buffer interface and resuspended in mitochondrial isolation buffer. The protein concentration of these isolated mitochondria was determined using the Bradford method.

Cell growth measurement. For the cell growth measurement, cells were seeded in three 6-cm-diameter dishes at 5×10^4 cells/dish. Cells were counted with a Neubauer chamber every day for 3 days. Until six passages after thawing, cells are considered in early passage; they are considered in late passage afterwards.

Apoptosis measurement by flow cytometry. For apoptosis measurement, cells were seeded in 6-cm-diameter dishes the day before treatment. Cells were incubated for 8 h with 16 μM actinomycin D in the presence or absence of caspase inhibitor z-VAD-FMK (100 μM). After treatment, apoptosis was detected using an allophycocyanin (APC)-conjugated annexin V staining kit (eBioscience, San Diego, CA) according to the manufacturer's instructions. The flow cytometry analyses were performed on a BD Accuri C6 flow cytometer (BD Bioscience).

Cellular ATP measurement. HeLa cells were plated at 2×10^4 cells/well in a 96-well plate the day prior to analysis. Cells were then incubated for 1 h in DMEM without glucose supplemented with 4 μM oligomycin or DMSO. ATP levels were determined using the ATP bioluminescence assay kit CLS II according to the manufacturer's instructions (Roche Applied Science). Luminescence was monitored in a Fluostar Optima plate reader luminometer (BMG Lab Technologies, Offenburg, Germany).

Oxygen consumption measurement. Oxygen consumption was measured with the MitoXpress kit (Luxel Biosciences Ltd., Cork, Ireland) accordingly to the manufacturer's instructions. Briefly, HeLa cells were grown in 96-well plates and incubated for 30 min with 10 μM FCCP and 20 μM rotenone or DMSO in culture medium without phenol red. After the addition of the probe, wells were sealed off with a layer of prewarmed heavy mineral oil and fluorescence was recorded for 2 h at 30°C on a FLEXstation (Molecular Devices, CA) using the time-resolved fluorescence mode.

Spectrophotometric assays for respiratory complexes. The measurement of the enzymatic activities of the individual complexes of the respiratory chain (RC) was performed by spectrophotometry (UVIKON 922 spectrophotometer; Kontron, Switzerland). Activities of complexes II, III, and IV were measured on total HeLa cell lysates. Activities of complexes I and V were measured on mitochondrion-enriched fractions. All samples were frozen and thawed three times before the assays, and assays were performed at RT. To normalize each complex activity, the citrate synthase activity of each sample was determined. A total of 20 to 60 μg of protein (determined by the Bradford method) was used to determine the activity of each complex. Citrate synthase and complex I, II, III, and IV activities were assayed according to the method of Spinazzi and colleagues (28). Complex V activity was measured as described by Kramarova and colleagues (29).

Complex I activity was measured at 340 nm using 60 μM ubiquinone as an acceptor and 100 μM NADH as a donor, in 50 mM potassium phosphate (pH 7.5) buffer containing 3 mg/ml of BSA and 300 μM KCN for 2 min. The addition of 10 μM rotenone allowed the quantification of the rotenone-sensitive activity.

Complex II activity was determined at 600 nm using 80 μM DCPIP and 20 mM succinate in a medium containing 25 mM potassium phosphate (pH 7.5), 1 mg/ml of BSA, and 300 μM KCN for 3 min. After 10 min of preincubation at 37°C, the reaction was started by 50 μM decylubiquinone. The oxidation of succinate was inhibited by 10 mM malonate.

Complex III activity was determined at 550 nm using 75 μM oxidized cytochrome *c* as an acceptor and 100 μM decylubiquinol as a donor in a medium containing 25 mM potassium phosphate (pH 7.5), 500 μM KCN, 100 μM EDTA, and 0.025% (vol/vol) Tween 20 for 2 min. The addition of 10 μg/μl of antimycin A allowed measurement of the specific complex III activity corresponding to the antimycin A-sensitive activity.

Complex IV activity was determined at 550 nm using 50 μM reduced cytochrome *c* in 50 mM potassium phosphate buffer (pH 7.0). The reaction was started by the addition of cell lysate (40 μg of proteins). The decrease in absorbance was observed for 3 min. KCN (300 μM) was used to check the specificity of complex IV activity.

Complex V (F_1F_0 ATPase) activity was determined by coupling the reaction to pyruvate kinase and lactate dehydrogenase. The oxidation of NADH was measured at 340 nm using 350 μM NADH in a medium containing 55 mM Tris (pH 8.0) buffer, 0.05% DDM, 20 mM $MgCl_2$, 50 mM KCl, 10 mM phosphoenolpyruvate, 30 μM antimycin A, 10 U of lactate dehydrogenase, and 5 U of pyruvate kinase. After incubation at 37°C for 5 min, the reaction was initiated with 2.5 mM ATP and monitored for 3 min. The F_1F_0 ATPase-specific activity was determined using 4 μM oligomycin.

The citrate synthase assay was performed at 412 nm to follow the reduction of 100 μM DTNB in the presence of 300 μM acetyl coenzyme A (acetyl-CoA) in 100 mM Tris (pH 8.0) and 0.1% (vol/vol) Triton X-100 medium. The reaction was started by 500 μM oxalacetic acid and monitored for 3 min.

Western blotting on whole-cell lysates. Cells were lysed with radioimmunoprecipitation assay (RIPA) buffer for 1 h on ice and centrifuged for 10 min at 18,000 × *g* to remove cellular debris. Cell extract proteins (40 μg) were loaded and run on a 12% SDS-PAGE gel. After electrophoresis, proteins were transferred to a PVDF membrane to be analyzed by immunoblotting using specific antibodies as indicated below. For Western blot

quantifications, band intensities obtained by ImageJ software were normalized to those obtained for sh control cells.

BN PAGE on isolated mitochondria. Isolated mitochondria were solubilized at 4°C during 30 min, either with 1 g of DDM/g of protein to solubilize individual complexes while preserving some interactions between complexes I, III, and IV or with 5 g of digitonin/g of protein to maintain SC. After centrifugation (5 min, 18,000 × *g*, and 4°C), solubilized mitochondrial proteins (40 μg) were loaded and run on a native PAGE Novex 3 to 12% bis-Tris gel (Life Technologies). For two-dimensional (2D) analysis, strips from the first-dimension blue native polyacrylamide gel electrophoresis (BN PAGE) were excised from the gel, incubated for 1 h at RT in 1% SDS and 100 mM β-mercaptoethanol, and then subjected to a 12% second-dimension denaturing gel electrophoresis (BN/SDS-PAGE). After electrophoresis, the gels were electroblotted onto PVDF membranes and probed with the desired antibodies. For Western blot quantifications, band intensities obtained by ImageJ software were normalized to those obtained for sh control cells.

TLC. Lipids were extracted from the mitochondrion-enriched fraction thanks to a modified form of the method of Bligh and Dyer (30), dissolved in chloroform, and resolved by thin-layer chromatography (TLC) on a silica gel 60 plate (Whatman, Maidstone, United Kingdom). For lipid migration, the plate was incubated in solvent containing chloroform, hexane, methanol, and acetic acid (50:30:10:5). After a drying step, lipids dots were colored by vapor of iodine crystals. Lipid dots were assigned on the basis of lipid standards loaded on the plate at the same time as samples. The quantification of CL and phosphatidylethanolamine (PE) spots were obtained by ImageJ software.

Phosphate content determination. Phosphate content of spots containing CL and PE on TLC plates was estimated by the method of Rouser and colleagues (31).

Analysis of CL composition by MS. CL species present in pellets of cells harvested at confluence were analyzed essentially as described previously (32). The relative abundances of the species in the sample extracts were determined by high-performance liquid chromatography (HPLC)-mass spectrometry (MS) using an Ultimate 3000 ultraperformance liquid chromatography (UPLC) system in conjunction with a Q Exactive Plus hybrid quadrupole-Orbitrap mass spectrometer (Thermo Finnigan Corporation, San Jose, CA). The MS was operated in the negative-ion heated electrospray ionization (HESI) mode.

Recombinant GST protein expression and purification. GST fusion proteins were expressed in BL21(DE3)pLys cells (Promega, Madison, WI). The bacteria were grown on LB medium containing 100 μg/ml of ampicillin and chloramphenicol, and the expression of fusion proteins was induced by 0.5 mM IPTG for 3 h at 30°C. The bacteria were pelleted and resuspended in 100 mM Tris-HCl (pH 7.6), 5 mM $MgCl_2$, 200 mM NaCl, 5 mM dithiothreitol (DTT), and 1% Triton X-100 with protease inhibitors. After sonication, cells debris were pelleted by centrifugation and the supernatants were incubated with glutathione-Sepharose beads. After several washing steps, GST fusion proteins were eluted with 20 mM glutathione in 100 mM Tris-HCl (pH 7.6) and 150 mM NaCl. The homogeneity and integrity of the recombinant proteins were checked by SDS-PAGE followed by Coomassie staining.

Lipid binding assay. Membrane lipid strips containing dots of 100 nmol of several lipids (P-6002; Echelon Biosciences Inc., Salt Lake City, UT) were probed with 0.5 μg of GST fusion proteins and analyzed by immunoblotting according to the manufacturer's instructions.

Electron microscopy. Cells were fixed with 2% glutaraldehyde in 0.1 M $NaPO_4$ buffer (pH 7.4) for 1 h. After three washing steps with 0.1 M $NaPO_4$ buffer (pH 7.4), cells were dehydrated, embedded in epoxy resin, and processed for electron microscopy as previously described (33). Ultrathin sections were finally contrasted with uranyl acetate and lead citrate and observed with a Technai 20 electron microscope (FEI Company, Eindhoven, The Netherlands).

Coimmunoprecipitation. The mitochondrion-enriched fractions were solubilized with DDM (2 g/g of protein), and the bc_1 complex and complex IV were immunoprecipitated using the bc_1 complex (ab109800) and complex IV (ab109801) immunocapture kits (Abcam) according to the manufacturer's instructions. Proteins were separated by gel electrophoresis on a 12% SDS-PAGE gel, transferred to a PVDF membrane, and immunoblotted with anti-UQCRFS1, anti-COX4, and anti-C11orf83 antibodies.

Statistical analysis. Graphing and data analysis were performed using GraphPad software (GraphPrism). All values are represented as means ± standard deviations (SDs) of values obtained in three independent experiments. Statistical significance (*P* value) was assessed by Student's *t* test.

Sequence analysis tools. BLASTP search was performed to find orthologs of C11orf83 (human) in the UniProtKB database version 15.14. Multiple-sequence alignment was performed using T-COFFEE (34) with the sequences of C11orf83 orthologs (UniProtKB [www.uniprot.org] sequence identifiers: Q6UW78, Q148G8, Q8K2T4, and Q2KP58). Secondary structures were predicted with PSIPRED (35), and the multiple-sequence alignment was edited using Aline (36). Functional domains and three-dimensional structure similarities were searched using InterPro (37) and HHPRED (38), respectively.

RESULTS

C11orf83 is an integral mitochondrial inner membrane protein facing the intermembrane space (IMS). C11orf83 is a protein of 10.1 kDa (93 amino acids [aa]) which is highly conserved in Metazoa. A similarity of 50% between human and *Xenopus laevis* protein sequences was determined using the sequence alignment presented in Fig. 1A and the BLOSUM64 matrix. In addition, secondary-structure prediction (PSIPRED) indicated the presence of conserved secondary structures (Fig. 1A). However, no obvious functional domain was found (InterPro), and no similarity to any protein with a resolved three-dimensional structure could be retrieved by HHPRED. Bioinformatic analysis, as well as a large-scale experimental study, originally predicted that C11orf83 was a secreted protein due to the presence of a potential signal peptide of 23 aa in length (Fig. 1A) (39, 40). However, C11orf83 was recently identified among the membrane proteins in a proteomic study of crude mitochondrial extracts from HeLa S3 cells (41). Therefore, we decided to analyze the localization of C11orf83 in HeLa cells by confocal microscopy and subcellular fractionation. As shown in Fig. 1B, C11orf83 colocalized with COX4, a mitochondrial protein. After Na_2CO_3 treatment of the mitochondrion-enriched fraction, membrane proteins, like TOMM20, were found in the pellet and soluble proteins, like DIABLO, were retained in the supernatant. C11orf83 was found in the membrane protein pellet (Fig. 1C), suggesting that it is a mitochondrial integral membrane protein, in agreement with the results of the proteomic study (41).

To determine C11orf83 membrane topology, we performed a proteinase K protection assay. Mitochondrion-enriched fractions from HeLa cells were treated with proteinase K in the presence or absence of saponin, which is used to permeabilize the mitochondrial outer membrane (OM). In contrast to the IM protein TIMM44, which is oriented toward the mitochondrial matrix, C11orf83 was digested by proteinase K in the presence of saponin, as was the case for DIABLO, a soluble protein from the IMS, and OPA1, a mitochondrial IM protein facing the IMS (Fig. 1D, lane 5). Taken together, these data indicate that C11orf83 is a mitochondrial IM protein facing the IMS. We performed the same assay using HeLa cells overexpressing the C-terminally V5-tagged form of C11orf83 (C11orf83-V5) and observed similar localization and membrane topology (see Fig. SA1A to C in the supplemental material).

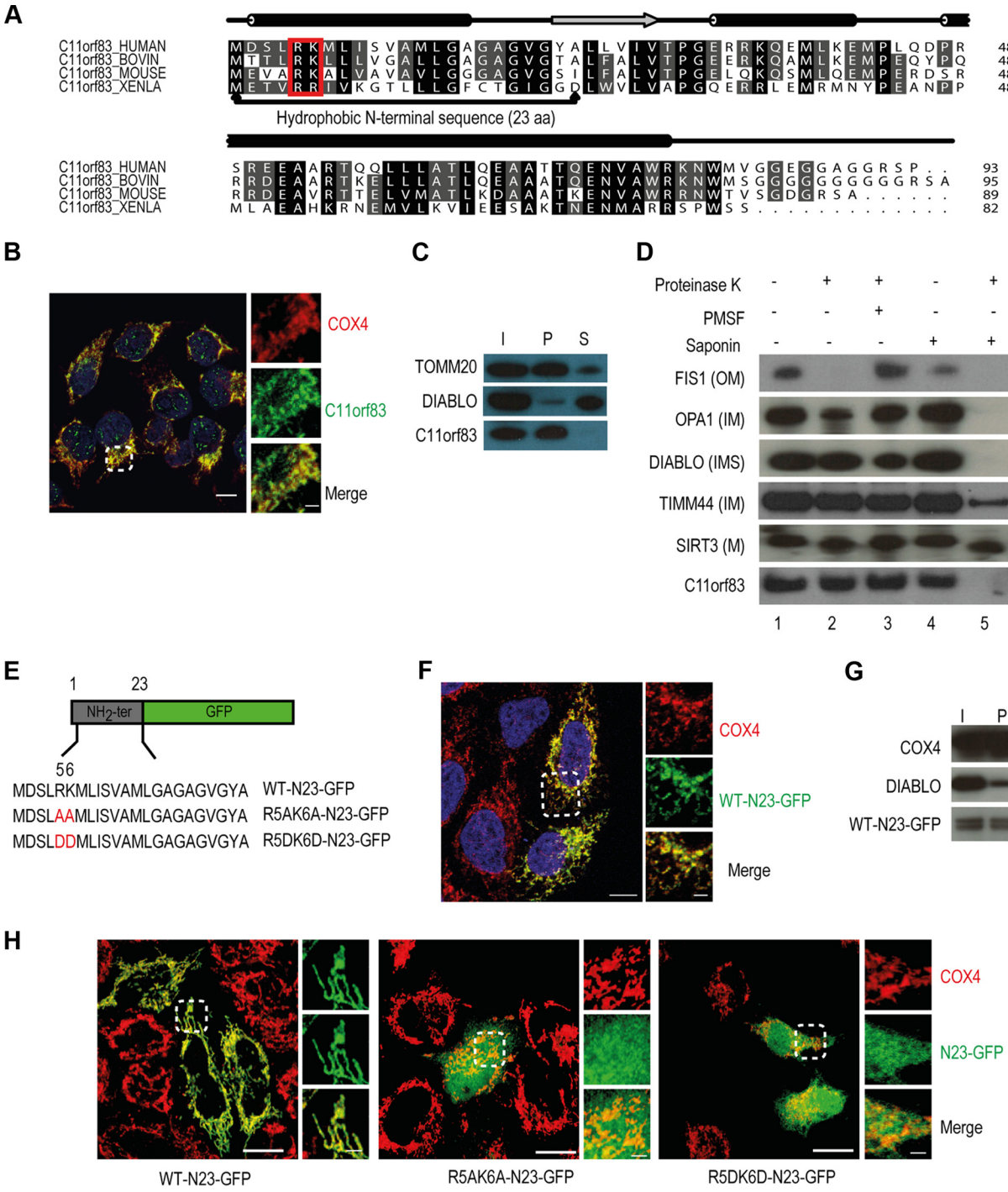

FIG 1 Subcellular localization of C11orf83 and identification of the membrane-anchoring sequence. (A) Sequence alignment of human C11orf83 with its orthologs. UniProtKB accession numbers of sequences are Q6UW78 (human), Q148G8 (bovine), Q8K2T4 (mouse), and Q2KP58 (*Xenopus laevis*). Predicted α-helices (cylinders) and β-strand (arrow) are displayed above the alignment. The conserved RK motif is highlighted by a red box. (B) Immunofluorescence analysis of C11orf83 localization in HeLa cells by confocal microscopy. Endogenous C11orf83 (anti-C11orf83 PAb [green]) was colocalized with COX4 (anti-COX4 PAb [red]). A merged color image is shown. (Scale bars: 10 μm in the large image and 2 μm in the small images.) (C) The mitochondrion-enriched fraction from HeLa cells was subjected to Na_2CO_3 extraction and analyzed by immunoblotting. C11orf83 and TOMM20 were retained in the insoluble membrane pellet (P), whereas the soluble protein DIABLO was released into the supernatant (S). I, input. (D) Mitochondrion-enriched fractions from HeLa cells were digested by proteinase K in the absence (lane 2) or presence (lane 5) of saponin and analyzed by immunoblotting. Control samples were analyzed in lanes 1, 3, 4, and 6. C11orf83 was only digested by proteinase K in the presence of saponin (lane 5), indicating that C11orf83 is in the IM and faces the IMS. M, matrix. (E) The NH_2-terminal part of C11orf83 (23 aa) was fused to GFP for expression in HeLa cells (WT-N23-GFP). Introduced mutations are shown in red in the corresponding sequences. (F) Immunofluorescence analysis of WT-N23-GFP localization in HeLa cells by confocal microscopy. WT-N23-GFP fusion protein was colocalized with COX4 (anti-COX4 PAb [red]). A merged color image is shown. (Scale bars: 10 μm in the large image and 2 μm in the small images.) (G) The mitochondrion-enriched fraction from HeLa cells transfected with WT-N23-GFP was subjected to Na_2CO_3 extraction and analyzed by immunoblotting. WT-N23-GFP (labeled with anti-GFP) and COX4 were retained in the insoluble membrane pellet (P). The minor band detected by the anti-GFP antibody may reflect protein degradation. (H) Immunofluorescence analysis of HeLa cells transfected with WT-N23-GFP or its mutated forms by confocal microscopy. The WT-N23-GFP fusion protein was colocalized with COX4 (anti-COX4 PAb [red]), whereas R5AK6A- and R5DK6D-N23-GFP fusion proteins were mislocalized in the cytosol. Merged color images are shown. (Scale bars: 10 μm in the large images and 2 μm in the small images, which are enlargements of the dashed boxes.)

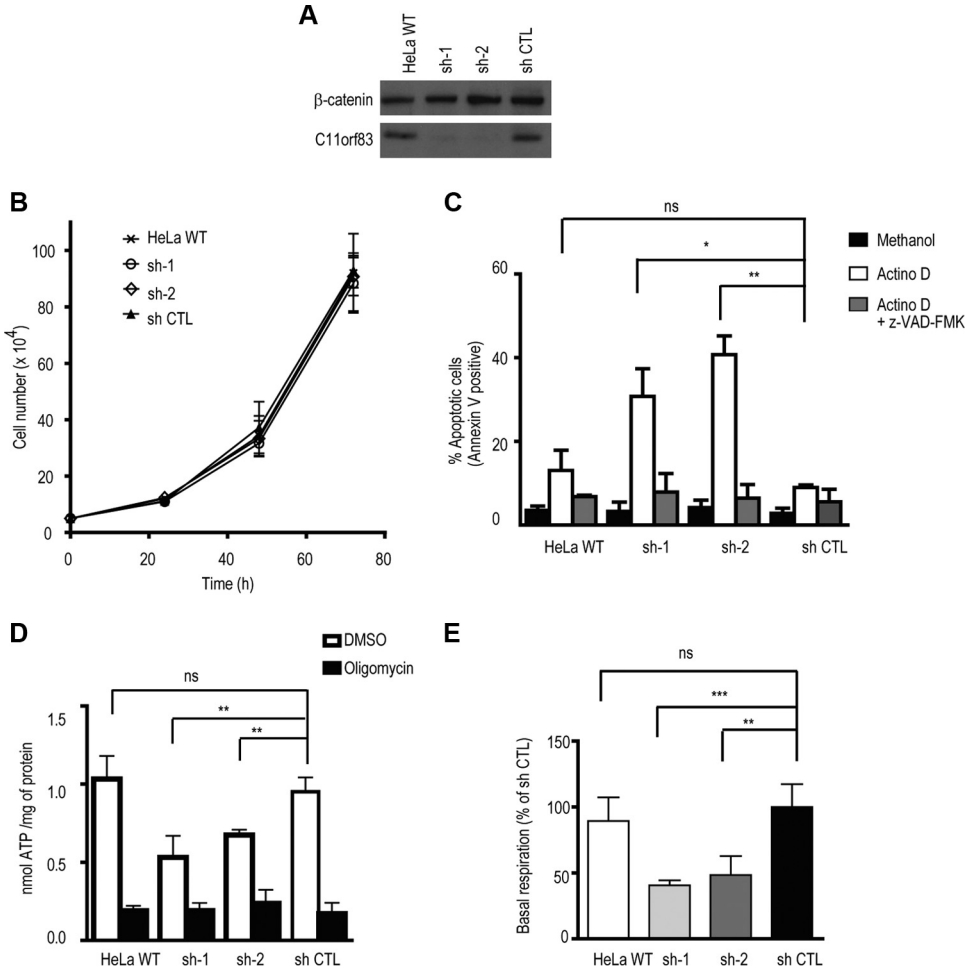

FIG 2 C11orf83 depletion in cell lines and its impact on mitochondrial functions. (A) Western blot analysis of HeLa cells downregulating C11orf83 (sh-1 and sh-2) compared to HeLa cells expressing a control shRNA (sh CTL) and to control HeLa cells without shRNA (HeLa WT). β-Catenin was used as a loading control. (B) Growth curve of HeLa WT, sh-1, sh-2, and sh CTL cells at early passages after thawing (mean ± SD [$n = 3$]). (C) Analysis of actinomycin D (Actino D)-induced apoptosis sensitivity of HeLa WT, sh-1, sh-2, and sh CTL cells. Cells were treated with Actino D or methanol (control) in the absence or presence of the caspase inhibitor z-VAD-FMK. Cell death was quantitated by flow cytometry using an annexin V-conjugated APC staining kit (mean ± SD [$n = 3$]). (D) Cellular ATP levels of HeLa WT, sh-1, sh-2, and sh CTL cells (mean ± SD [$n = 3$]). Before the ATP assay, cells were cultured in a medium without glucose in the presence of oligomycin (to confirm the specificity of the assay by inhibiting ATP synthesis) or DMSO (as a control). (E) Analysis of the basal respiration of HeLa WT, sh-1, sh-2, and sh CTL cells. Results are expressed as the means ± SDs of percentages of the basal respiration of sh CTL cells ($n = 3$). *, $P < 0.05$; **, $P < 0.01$; ***, $P < 0.001$; ns, not significant.

Therefore, we hypothesized that the hydrophobic N-terminal part of C11orf83, predicted to be a secretory signal peptide (39, 40), would instead serve as a mitochondrial targeting signal and a membrane-anchoring region. To test this hypothesis, we expressed a modified form of GFP with this peptide fused at its N terminus (WT-N23-GFP) in HeLa cells. By confocal microscopy, we observed a clear colocalization of the mitochondrial COX4 signal with the WT-N23-GFP signal (Fig. 1E and F). The mitochondrion-enriched fraction from HeLa cells expressing WT-N23-GFP was then subjected to Na_2CO_3 treatment. WT-N23-GFP was found in the pellet corresponding to the membrane protein fraction (Fig. 1G). These data suggest that this N-terminal sequence is sufficient to target and anchor C11orf83 to the mitochondrial IM. We identified a conserved RK motif in this N-terminal region (Fig. 1A, red box). We replaced these 2 residues either with alanine or with aspartic acid (Fig. 1E) and analyzed the localization of these mutated N23-GFP forms in HeLa cells. Mutations in the RK motif abrogated N23-GFP targeting to the mitochondria and induced a cytoplasmic localization (Fig. 1H). We observed similar results with RK-mutated C11orf83-V5 (see Fig. SA1D and E in the supplemental material), which confirmed the key role of these two conserved and positively charged amino acids for the correct mitochondrial localization of C11orf83.

C11orf83 downregulation impairs mitochondrial functions. To investigate the biological function of C11orf83 at the cellular level, we engineered HeLa cell lines by stably downregulating C11orf83 using shRNA technology. Two cells lines, called sh-1 and sh-2, were chosen due to their absence of detectable C11orf83 protein expression (Fig. 2A). We noticed that C11orf83 downregulation was more stable in sh-2 cells than in sh-1 cells (data not shown). On freshly thawed cell lines (less than six passages), we observed similar growth curves for cells downregulating C11orf83 and controls (Fig. 2B). However, we noticed that after six passages, C11orf83-deficient cells showed a significantly reduced cell

TABLE 1 Enzymatic activities of mitochondrial RC complexes in WT, sh control, and C11orf83-deficient cells (sh-1 and sh-2)[a]

Complex	Enzymatic activity in indicated cell type			
	HeLa WT	sh-1	sh-2	sh CTL
I	26.4 ± 1.6	20.1 ± 1.0*	17.2 ± 2.9**	31.3 ± 1.9
II	7.8 ± 3.5	4.8 ± 1.5*	4.0 ± 1.0**	8.7 ± 1.8
III	94.0 ± 13.9	62.5 ± 23.4*	70.9 ± 23.7*	128.2 ± 46.0
IV	100.1 ± 13.0	61.2 ± 8.8*	79.9 ± 3.5*	121.7 ± 21.3
V	25.8 ± 6.5	13.4 ± 5.6*	10.6 ± 0.3*	28.3 ± 10.4

[a] Values are normalized to citrate synthase activities and reported as means ± SDs (n = 3). *, $P < 0.05$; **, $P < 0.01$ (compared to sh CTL values).

growth compared to that of controls (see Fig. SA2 in the supplemental material). These data suggest that the C11orf83 loss has a potential impact on resistance to *in vitro* cellular aging.

Since C11orf83 was shown to be mitochondrial and several studies proposed a connection between aging and mitochondria dysfunctions (42–46), a deeper analysis of the impact of C11orf83 depletion on mitochondrial physiology was performed. To comply with the instructions of the American Type Culture Collection (ATCC) (47), which recommend the use of cell lines within five passages to ensure reliable and reproducible results, all the following experiments were performed with freshly thawed cells. As mitochondria play a key role in apoptosis and ATP production, we first monitored the sensitivities of these cell lines to actinomycin D-induced apoptosis, as well as their ATP levels. Upon actinomycin D treatment, we observed a significant increase in annexin V-positive cells among C11orf83-deficient cells by flow cytometry analysis (Fig. 2C). The assay specificity was confirmed by the inhibition of annexin V staining in the presence of z-VAD-FMK, a pan-caspase inhibitor. These results showed that the knockdown of C11orf83 induced a higher sensitivity to this apoptotic stimulus. Next, we measured the ATP level of each cell line using a luciferase reporter assay. The C11orf83-deficient cell lines sh-1 and sh-2 showed 40% and 30% reductions in ATP levels compared to controls, respectively (Fig. 2D). Since the cellular ATP is mainly provided by mitochondria via the ETC, we wondered if the observed decrease in cellular ATP could be due to an impaired respiration. Using a cell-based assay, we showed that the loss of C11orf83 induced a significant decrease of basal respiration (Fig. 2E). Taken together, these results suggest that C11orf83 is important for proper mitochondrial physiology.

C11orf83 depletion induces defects in respiratory SC. As the loss of C11orf83 induced a decrease in basal respiration, we investigated its potential effects on individual RC complexes. In Table 1, we summarize the activities of the five RC complexes in knockdown and control cells measured by spectrophotometry analysis. All complexes in C11orf83 knockdown cells demonstrated a significantly lower activity than in controls.

Then, we examined the effects of C11orf83 downregulation on the steady-state levels of proteins that form ETC complexes. Immunoblotting on whole-cell lysates, under denaturing conditions, showed that the loss of C11orf83 did not affect the amount of representative subunits for each complex (NDUFV2 for complex I, SDHB for complex II, UQCRC1 for bc_1 complex, COX4 for complex IV, and ATP5B for complex V) (Fig. 3A).

To determine whether the assembly of ETC complexes and SC was affected in C11orf83-depleted cells, we performed blue native (BN) gel electrophoresis followed by immunoblotting on isolated mitochondria solubilized by DDM. Under this condition, complexes II and V were extracted as individual complexes (visualized with antibodies against SDHB for complex II and ATP5B for complex V) (Fig. 3B). Complexes I and IV and the bc_1 complex dimer were also extracted as individual complexes and additionally found as III_2/IV, I/III_2, and I/III_2/IV SC (visualized with antibodies against NDUFB6 for complex I, UQCRC1 for bc_1 complex, and COX4 for complex IV) (Fig. 3C). C11orf83 depletion caused no apparent change in the detectable amounts of complexes I, II, III_2, IV, and V and of the I/III_2 SC (Fig. 3B and C). In contrast, we observed a significant reduction in the amounts of the I/III_2/IV and III_2/IV SC, with a more pronounced effect for the III_2/IV SC (Fig. 3C, D, and E).

C11orf83 interacts with the bc_1 complex and is involved in the early stages of bc_1 assembly. To determine the cause of the reduced amounts of the I/III_2/IV and III_2/IV SC, we solubilized mitochondria using digitonin, which better preserves SC integrity than DDM, and performed two-dimensional (2D) BN/SDS-PAGE followed by immunoblotting. When this protocol was applied to control cells, complex I (visualized with antibody against NDUFV2) was found uniquely in the I/III_2/IV SC, whereas complexes IV and III_2 (visualized with antibodies against COX4 and UQCRC1, respectively) were found both as individual complexes and in the III_2/IV and I/III_2/IV SC, as expected from the literature (16, 48) (Fig. 4A). In mitochondria from sh-2 cells solubilized with digitonin, UQCRC1 was predominantly found in the I/III_2/IV SC, and we observed a significant reduction in the amounts of complex III_2 and the III_2/IV SC (Fig. 4A, arrows, and B and C). This observation suggests that complex I sequesters the limited amount of assembled complex III_2 and the III_2/IV SC available in sh-2 cells, similarly to what was reported for other assembly defects of the bc_1 complex (18) or complex IV (17). The fact that we could observe free bc_1 complex as well as the III_2/IV SC in DDM-solubilized mitochondria from C11orf83-depleted cells (Fig. 3C) was probably due to the dissociation of the I/III_2/IV SC under these extraction conditions. Taken together, our data indicate that the loss of C11orf83 induces a deficiency in bc_1 complex assembly.

To further analyze this bc_1 complex assembly deficit in C11orf83-depleted cells, we immunoblotted two other bc_1 complex subunits: UQCRB and CYC1 (Fig. 4A). These subunits were chosen according to the literature which describes bc_1 complex assembly in yeast. In the current model, the Qcr7p/Qcr8p/Cytbp subcomplex, called the bc_1 core complex, interacts sequentially with two other preformed subcomplexes, Cyt1p/Qcr6p/Qcr9p and Cor1p/Qcr2p, to form intermediate complexes. The late stages of bc_1 complex assembly correspond to the incorporation of Rip1p and Qcr10p and the dimerization of the full complex (5, 6). Therefore, by selecting UQCRC1 (human ortholog of Cor1p), UQCRB (human ortholog of Qcr7p), and CYC1 (human ortholog of Cyt1p), we can study the three potential subcomplexes involved in the early stages of bc_1 complex assembly. Using antibodies against UQRCB and CYC1, we observed a clear decrease in the bc_1 complex and the III_2/IV SC in C11orf83-depleted cells, which is in agreement with the results obtained with the anti-UQCRC1 antibody (Fig. 4A). At lower molecular weights, we noticed an additional accumulation of complex intermediates containing CYC1 but not UQCRC1 or UQCRB, presumably equivalent to the Cyt1p/Qcr6p/Qcr9p subcomplexes (Fig. 4A, arrow, and D). Importantly, overexpression of a C11orf83-V5 form (translated from

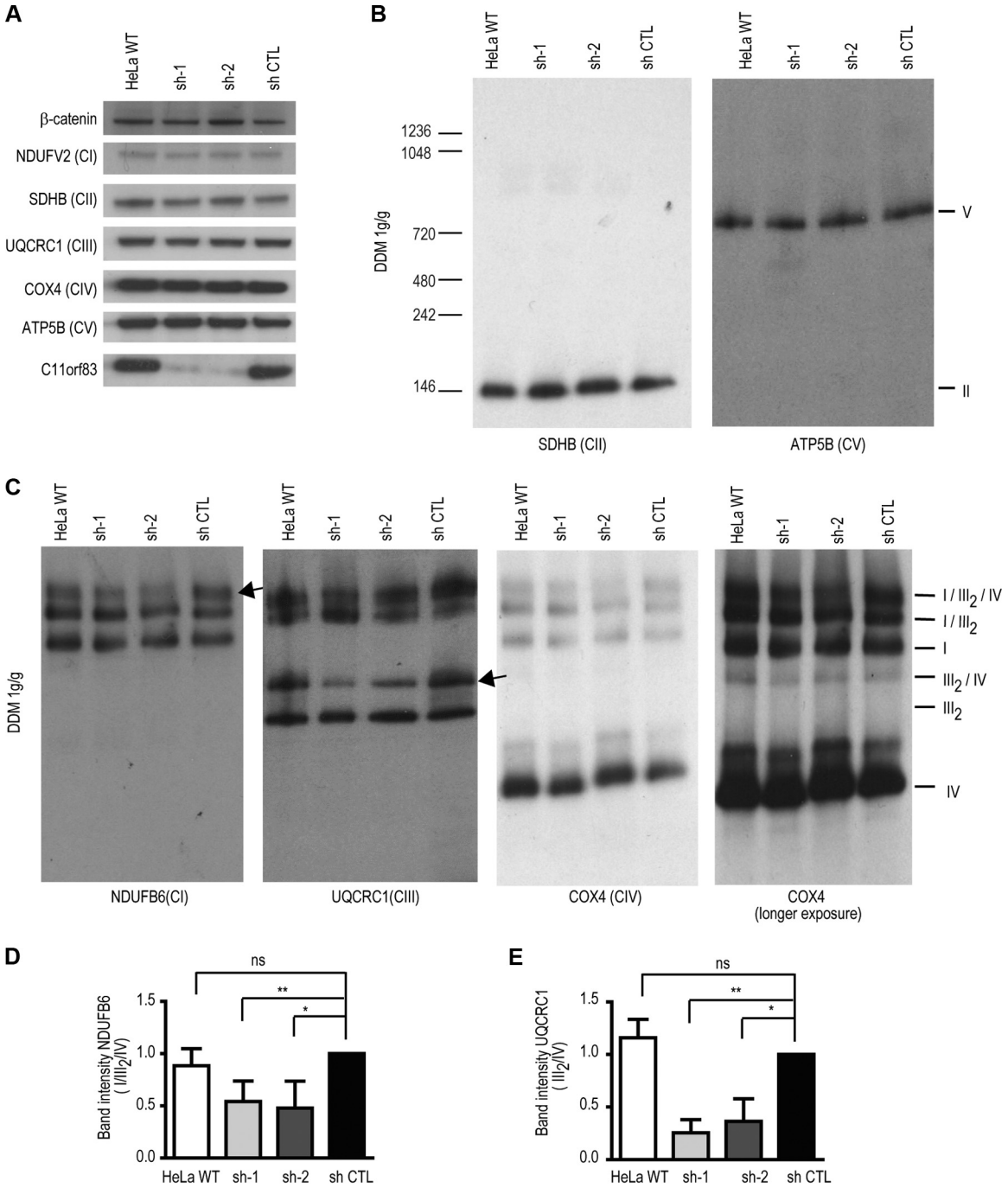

FIG 3 C11orf83 depletion induces defects in the respiratory SC. (A) Western blot analysis of the steady-state levels of representative subunits of RC complexes (NDUFV2 for complex I [CI], SDHB for complex II [CII], UQCRC1 for the bc_1 complex [CIII], COX4 for complex IV [CIV], and ATP5B for complex V [CV]) in HeLa WT, sh-1, sh-2, and sh CTL cells. β-Catenin was used as a loading control. (B to E) Analysis of the assembly of RC complexes and SC. (B and C) DDM-solubilized isolated mitochondria from HeLa WT, sh-1, sh-2, and sh CTL cells were analyzed by BN PAGE and immunoblotted using antibodies against RC complexes. Differences between cells lines are shown by arrows. (D) Quantification of the I/III_2/IV SC using antibody against NDUFB6 (mean ± SD [$n = 3$]). (E) Quantification of the III_2/IV SC using antibody against UQCRC1 (mean ± SD [$n = 3$]). *, $P < 0.05$; **, $P < 0.01$; ns, not significant.

an mRNA which is not targeted by the shRNA) in sh-2 cells clearly decreased the accumulation of CYC1-containing complex intermediates (Fig. 4E and F). This result confirms that C11orf83 is an assembly factor involved in the early stages of bc_1 complex assembly.

We next studied the effect of C11orf83 deletion on the steady-state levels of several bc_1 complex subunits by performing immunoblotting on whole-cell lysates under denaturing conditions. We observed a pronounced reduction in the UQCRB (human ortholog of Qcr7p) (Fig. 5A and B) level and a slight reduction in the UQCRQ (human ortholog of Qcr8p) (Fig. 5A and C) level in C11orf83-depleted cells, suggesting a reduction in the amount of the bc_1 core complex. The protein levels of all other analyzed

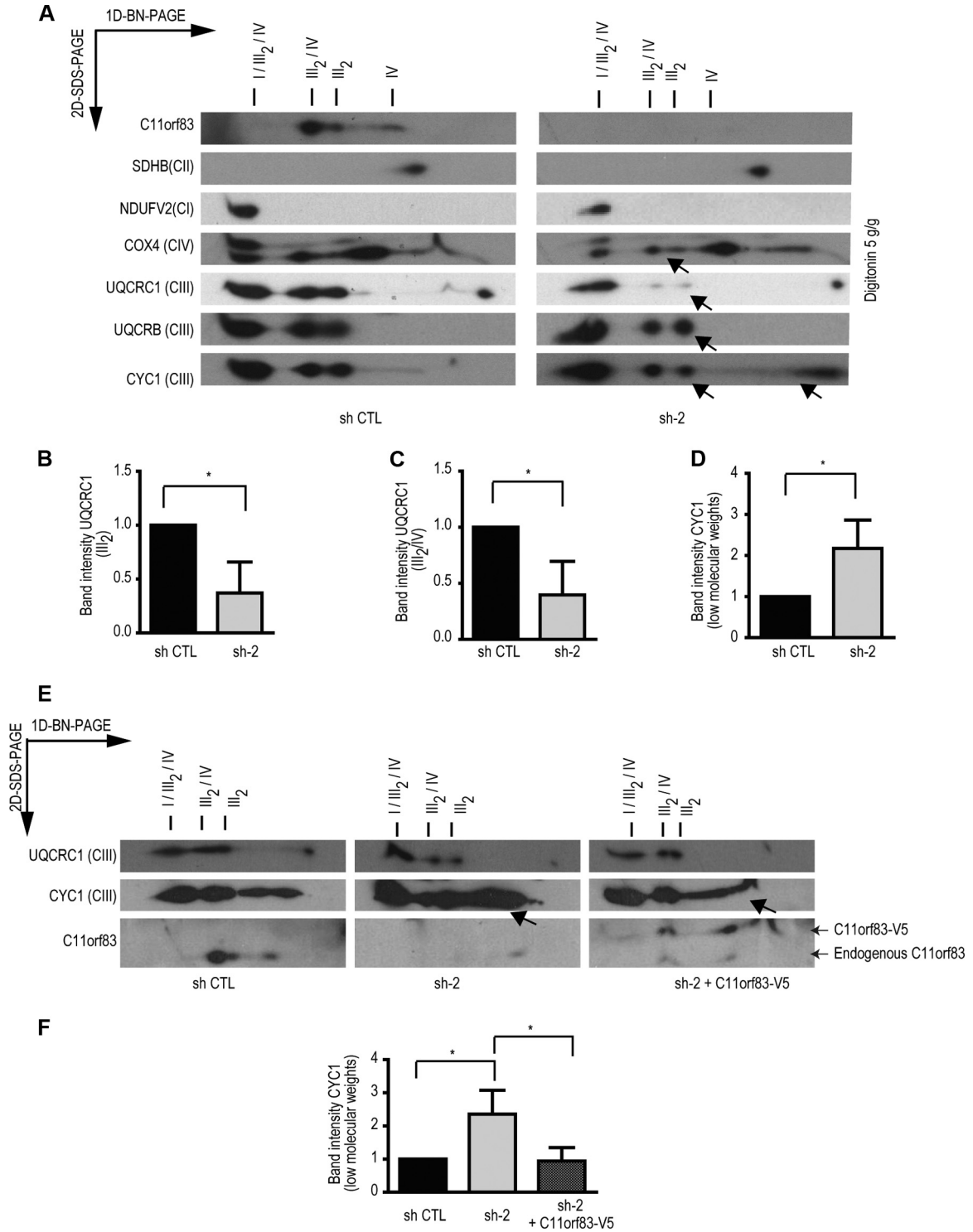

FIG 4 C11orf83 is involved in bc_1 complex assembly. (A to D) Digitonin-solubilized isolated mitochondria from sh CTL and sh-2 cells were analyzed by 2D BN/SDS-PAGE. (A) The bc_1 complex was detected with antibodies against UQCRC1, UQCRB, and CYC1. Antibodies against NDUFV2, SDHB, and COX4 were used to detect complexes I, II, and IV, respectively. SDHB was used as a loading control since complex II assembly was shown to be unaffected by C11orf83 depletion and C11orf83 as a control for downregulation (Fig. 3B). Quantification of complex III_2 (B) and the III_2/IV SC (C) was performed using antibody against UQCRC1. Quantification of CYC1-containing complex intermediates at low molecular weights was performed using antibody against CYC1 (D). Values are means ± SDs ($n = 3$). (E) Digitonin-solubilized isolated mitochondria from sh CTL cells, sh-2 cells, and sh-2 cells transfected with C11orf83-V5 were analyzed by 2D BN/SDS-PAGE. The bc_1 complex was detected with antibodies against UQCRC1 and CYC1. The presence of endogenous C11orf83 or its V5-tagged form was detected by using an antibody against C11orf83. (F) Quantification of the CYC1-containing complex intermediates at low molecular weights using antibody against CYC1 (mean ± SD [$n = 3$]). *, $P < 0.05$.

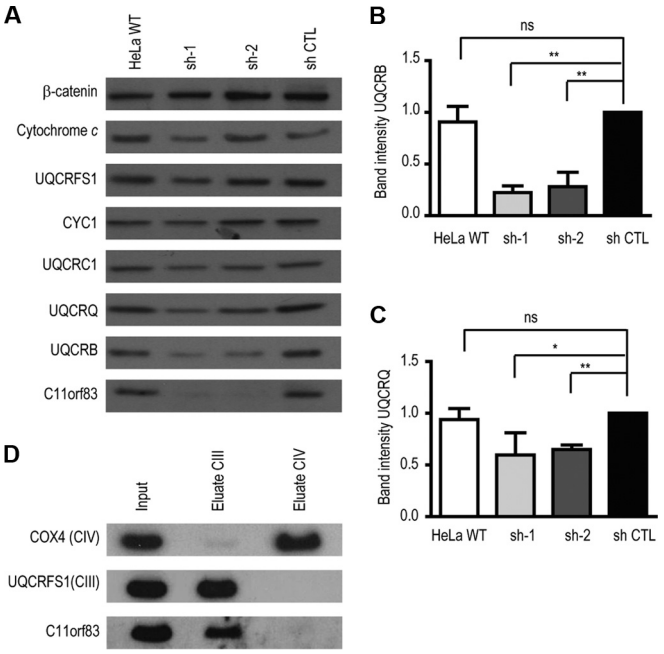

FIG 5 C11orf83 interacts with the bc_1 complex and is involved in the stabilization of its subunits UQCRQ and UQCRB. (A to C) Western blot analysis of the amount of several bc_1 complex subunits in whole-cell lysates from HeLa WT, sh-1, sh-2, and sh CTL cells under denaturing conditions. β-Catenin was used as a loading control and C11orf83 as a control for downregulation. UQCRB and UQCRQ protein levels were quantified using antibodies against UQCRB (B) and UQCRQ (C). Values are means ± SDs ($n = 3$). (D) Coimmunoprecipitation analyses. The bc_1 complex and complex IV were immunoprecipitated from DDM-solubilized HeLa WT mitochondrion-enriched fractions. Western blot analysis was performed after SDS-PAGE using anti-COX4 for complex IV (CIV), anti-UQCRFS1 for the bc_1 complex (CIII), and anti-C11orf83. *, $P < 0.05$; **, $P < 0.01$; ns, not significant.

subunits were not modified compared to controls (Fig. 3A and 5A). Therefore, C11orf83 seems to be specifically involved in the stabilization of the bc_1 core complex at the early stage of bc_1 complex assembly. The accumulation of the CYC1-containing complex intermediates observed in the absence of C11orf83 (Fig. 4A) could be due to limiting amounts of the bc_1 core complex.

As we showed that C11orf83 is involved in bc_1 complex assembly, we wanted to check whether it interacts with this complex. A first indication came from the 2D BN/SDS-PAGE, in which C11orf83 was detected in bands migrating at the same molecular weights as complexes IV and III_2 and the III_2/IV SC (Fig. 4A). These observations indicate that C11orf83 could interact with bc_1 complex and with complex IV. To test this hypothesis, we conducted coimmunoprecipitation experiments. The bc_1 complex and complex IV were successfully immunoprecipitated from HeLa wild-type (WT) mitochondrion-enriched fractions solubilized using DDM, as shown by Western blot analysis using antibodies against UQCRFS1 and COX4, respectively (Fig. 5D). C11orf83 was specifically copurified with the bc_1 complex, which indicates that C11orf83 interacts with this complex. Under these conditions, we did not detect any interaction between C11orf83 and complex IV (Fig. 5D).

C11orf83 is a CL-binding protein involved in crista maintenance. Phospholipids, in particular CL, the mitochondrion-specific phospholipid, are essential for the stabilization and function of the bc_1 complex (49) as well as for the stabilization of the III_2/IV_2 SC in yeast (50) and the III_2/IV and I/III_2/IV SC in mammalian cells (51, 52). As we have observed a bc_1 complex deficiency with an impaired formation of the III_2/IV SC in C11orf83-deficient cells, we hypothesized that C11orf83 could either be involved in phospholipid metabolism or interact with mitochondrial phospholipids. Therefore, we studied the lipid composition of mitochondrion-enriched fractions from either sh-2 or control cells by TLC. Mitochondrial fractions from both cell lines displayed similar levels of CL, phosphatidylethanolamine (PE), phosphatidylinositol (PI), and phosphatidylcholine (PC). They had equivalent CL-to-PE ratios, both when measuring TLC spot intensity (sh CTL, 0.71 ± 0.11; sh-2, 0.67 ± 0.13) and when measuring phosphate content (sh CTL, 0.23 ± 0.03; sh-2, 0.15 ± 0.05) (Fig. 6A). Quantification of total CL in both cell lines by MS confirmed this result (sh CTL, 1.4 ± 0.2 nmol/mg of protein; sh-2, 1.8 ± 0.4 nmol/mg of protein). CL has four acyl chains which can vary in length and unsaturation. Further analysis of mass spectra to evaluate CL acyl composition revealed that some CL species of the C_{64} ($4\times C_{16}$), C_{66} ($3\times C_{16}$ and $1\times C_{18}$), and C_{68} ($2\times C_{16}$ and $2\times C_{18}$) clusters were significantly increased in sh-2 cells ($C_{64:4}$, $C_{66:5}$, $C_{66:6}$, $C_{68:5}$, $C_{68:6}$, and $C_{68:7}$) (Fig. 6B and C). However, there was no shift in unsaturation, only an increase in the abundance of the C16-enriched CL clusters. Our results indicate that the depletion of C11orf83 induces a shift in the CL composition of mitochondria to shorter acyl chains.

To analyze the potential binding of C11orf83 to mitochondrial phospholipids, we monitored the direct interaction of recombinant GST-C11orf83 protein on phospholipid blots (53). While recombinant GST did not produce any signal in this assay, GST-C11orf83 specifically bound to CL, PA, and sulfatide (Fig. 7 A). C11orf83 binding to sulfatide, a sphingolipid, is most probably not physiologically relevant, as this lipid is not known to be present in mitochondria but is found in the plasma membrane in most eukaryotic cells (54). In contrast, C11orf83 may physiologically interact with CL and/or with PA, which is synthesized in the mitochondrial OM and transferred in the IM to be converted to CL (55). To determine the CL-binding domain of C11orf83, we generated recombinant GST proteins corresponding to several subportions of C11orf83 and observed their potential interaction with phospholipids. GST-Δ23C11orf83, C11orf83 protein depleted of its N-terminal transmembrane domain, showed binding to CL, PA, and sulfatide similar to that shown by full-length C11orf83 (Fig. 7B and C), indicating that interaction with CL is not mediated by the C11orf83 membrane-anchoring domain. As most of CL-binding proteins interact with CL by their helices (56–59), we analyzed the phospholipid binding abilities of predicted C11orf83 helices, either separately (GST-helix 2 and GST-helix 3) or together (GST-helix 2-helix 3) (Fig. 7B and C). Fusion proteins GST-helix 2 and GST-helix 3 did not produce any signal in this assay, in contrast to the protein GST-helix 2-helix 3, which displayed a binding to CL, PA, and sulfatide similar to that of GST-C11orf83 (full length) (Fig. 7C). Taken together, our experiments showed that the combination of helix 2 and helix 3 (aa 23 to 80) is necessary and sufficient for CL binding (Fig. 7B) and could play a role in the CL binding of the bc_1 complex and/or in III_2/IV SC stabilization.

Recently, Cogliati and colleagues showed that crista morphology is linked to the assembly and stability of respiratory SC

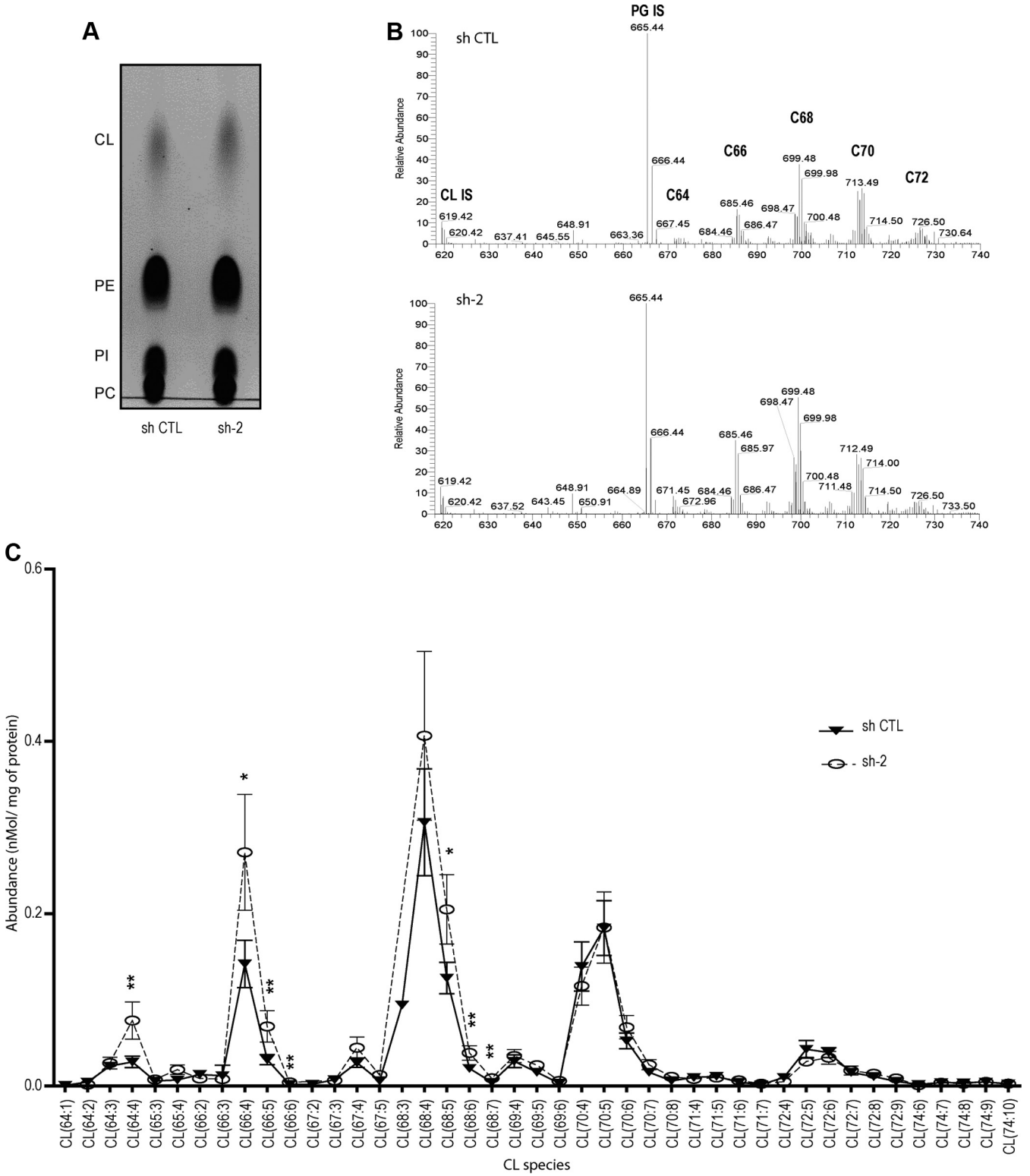

FIG 6 C11orf83 loss induces changes in fatty acid CL composition (A) TLC analysis of the lipid compositions of mitochondrion-enriched fractions from sh-2 or sh CTL cells. (B) Representative CL mass spectra from sh CTL and sh-2 cells. The different CL clusters are indicated using CXX (where the number "XX" designates the amount of carbon atoms in the fatty acid side chains). *m/z* 619.4 and *m/z* 665.4 are the CL and phosphatidylglycerol (PG) internal standards, respectively. (C) Quantification of CL species in sh-2 and sh CTL cells (mean ± SD [$n = 4$]). CL species are represented as CL(XX:Y), where XX designates the total amount of carbon atoms and Y corresponds to the total number of double bonds in the fatty acid side chains. There is a subtle but significant increase in the abundance of the C_{64}, C_{66}, and C_{68} clusters. *, $P < 0.05$; **, $P < 0.01$.

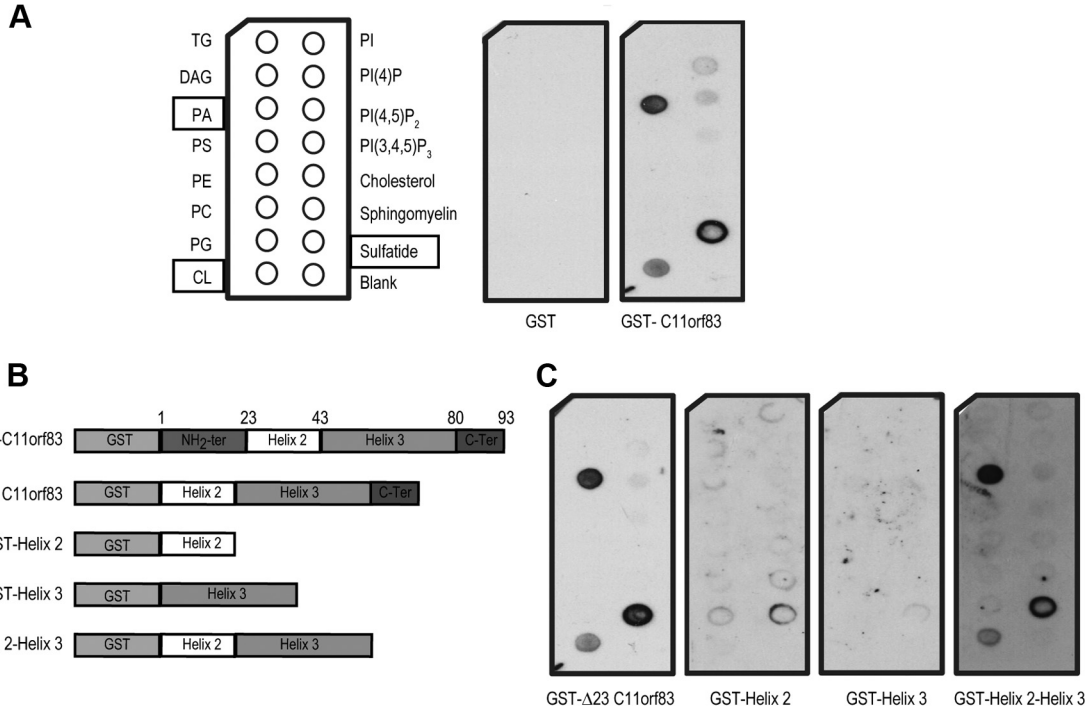

FIG 7 C11orf83 is a CL-binding protein. (A) Recombinant GST-C11orf83 was used to probe membrane lipid strips. Recombinant GST was used as a control of nonspecific binding. (B) Schematic representation of the different GST fusion proteins of full-length and truncated C11orf83, with amino acid numbering. (C) Lipid binding assays of GST-Δ23C11orf83, GST-helix 2, GST-helix 3, and GST-helix 2-helix 3. TG, triglyceride; DAG, diacylglycerol; PS, phosphatidylserine; PG, phosphatidylglycerol; PI(4)P, phosphatidylinositol-4-phosphate; PI(4,5)P, phosphatidylinositol-4,5-phosphate; PI(3,4,5)P, phosphatidylinositol-3,4,5-phosphate).

(60). Since we observed defects in bc_1 complex-containing SC in the absence of C11orf83, we suspected modifications in the IM morphology. Using electron microscopy, we confirmed a disorganization of the IM ultrastructure and crista architecture in C11orf83-depleted cells compared to control cells (Fig. 8A). This observation is strikingly similar to what was reported with cells depleted for OPA1, a GTPase with the same localization and topology as C11orf83 (61–63). In addition, C11orf83-deficient cells present several features which are similar to those observed in OPA1-downregulating cells, including impaired respiration, decreased ETC enzymatic activities, and high apoptosis sensitivity (62, 63) (Fig. 2C and E; Table 1). Because OPA1 was shown to be involved in high-molecular-weight complexes (60), we analyzed whether C11orf83 depletion induced changes in mitochondrial OPA1-containing complexes. Figure 8B shows the migration pattern of OPA1 in C11orf83 depleted cells compared to sh control cells in 2D BN/SDS-PAGE. Whereas OPA1 was found in complexes of the expected size of around 480 and 720 kDa in control cells (60), OPA1 was aberrantly localized in complexes of various molecular masses in C11orf83-depleted cells. As OPA1 is located in the crista junction and forms a molecular bridge between the adjacent membranes of the cristae (64), the formation of aberrant complexes containing OPA1 may be due to the disorganization of the IM ultrastructure observed in C11orf83-deficient cells (Fig. 8B).

C11orf83 is cleaved by OMA1 upon mitochondrial stress, like OPA1. OPA1 is known to undergo proteolytic processing by several proteases, either constitutively or upon mitochondrial depolarization (65–68). For example, under stress conditions induced by CCCP, OPA1 is cleaved and inactivated by the zinc metalloprotease OMA1 (67, 68), which consequently promotes mitochondrial fragmentation. It was reported that C11orf83 was degraded upon exposure to CCCP in parkin-overexpressing cells (69). Therefore, we compared the proteolytic processing of C11orf83 and OPA1 in HeLa cells that do not overexpress parkin under different stress conditions that induce mitochondrial membrane potential ($\Delta\Psi$) loss, ATP loss, reactive oxygen species production, or transmembrane pH gradient (ΔpH) loss. We showed, by Western blot analysis, that both C11orf83-V5 and OPA1 are specifically degraded upon stresses that induce $\Delta\Psi$ loss (CCCP, valinomycin, and FCCP) (Fig. 9A). We performed a protease inhibitor screening to identify the enzyme(s) responsible for C11orf83 degradation. C11orf83-V5 degradation was impaired by O-PHE, an inhibitor of metalloproteases, and to a lesser extent by DCI, an inhibitor of serine proteases (Fig. 9B). Since OMA1 is known to cleave OPA1 upon CCCP-induced stress, we downregulated OMA1 expression using siRNA and analyzed the proteolysis of C11orf83-V5 in the presence or absence of CCCP. In the absence of CCCP, the OMA1 siRNA did not modify the C11orf83-V5 protein level. However, upon CCCP stress, we observed that OMA1 downregulation was correlated with a reduction in C11orf83-V5 degradation (Fig. 9C). The residual C11orf83-V5 proteolysis might be due to residual OMA1 protein (around 20%) unaffected by the siRNA treatment or to DCI-sensitive serine proteases as hinted by the protease inhibitor screening assay. The same experiment performed on endogenous C11orf83 instead of overexpressed C11orf83-V5 confirmed that C11orf83 is a target of OMA1 upon mitochondrial depolarization (see Fig. SA3 in the supplemental mate-

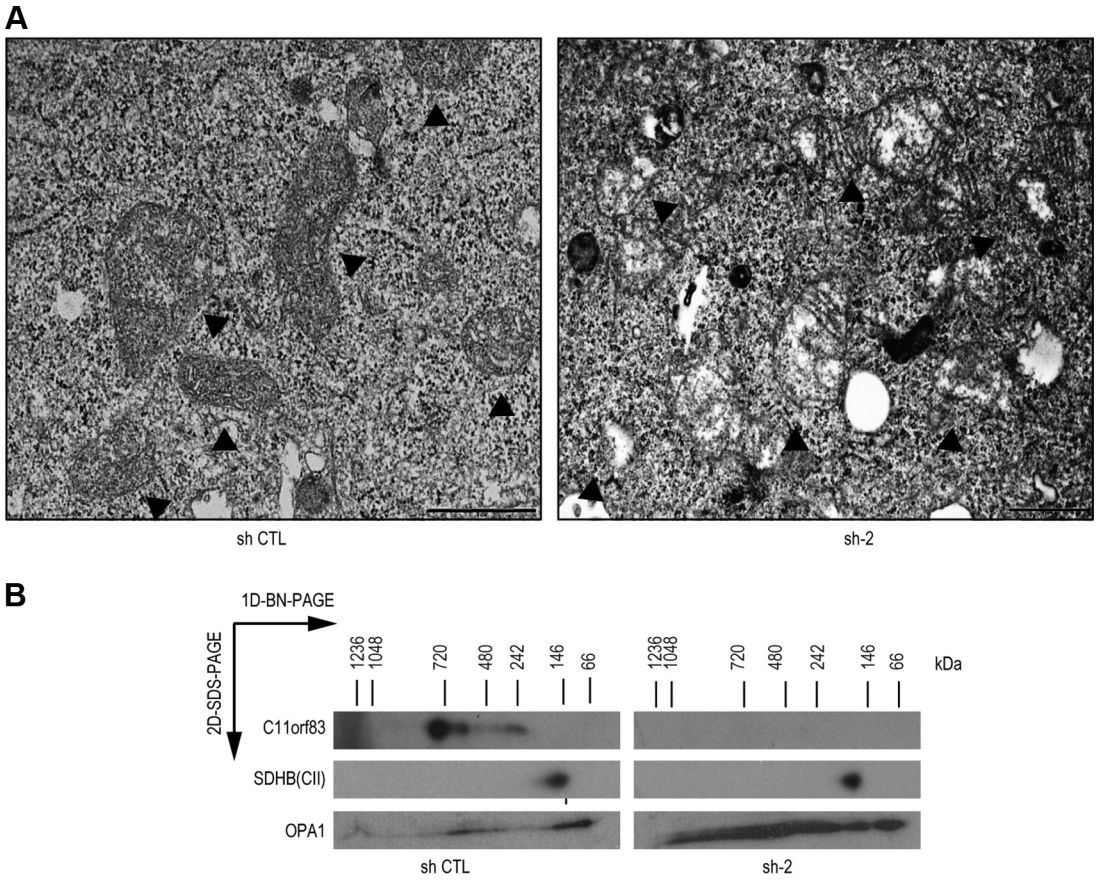

FIG 8 C11orf83 is involved in crista maintenance. (A) Electron microscopy micrograph of thin sections of sh CTL (left) and sh-2 (right) cells showing the ultrastructure of mitochondria. Arrowheads indicate mitochondria. (Scale bars: 1 μm.) (B) Analysis of OPA1-containing complexes in sh CTL and sh-2 cells. Isolated mitochondria were solubilized by digitonin and analyzed by 2D BN/SDS-PAGE. Western blot analysis was performed using antibodies against C11orf83 to control the downregulation, SDHB for the loading control, and OPA1.

rial). In contrast to data reported by Head and colleagues, we were not able to recover the long OPA1 isoforms with siRNA against OMA1 (67). This observation can be explained by the incomplete OMA1 downregulation and/or by the absence of L-OPA1 overexpression in our experiment. Altogether, these data confirm that C11orf83, like OPA1, plays a key role in crista structure maintenance by allowing proper assembly of the bc_1 complex and SC stabilization and that it may be regulated by OMA1 activity.

DISCUSSION

In this study, we have identified C11orf83, a previously uncharacterized human protein, as an integral mitochondrial IM protein facing the IMS. We have established that the N-terminal part (aa 1 to 23) of this protein is responsible for its targeting and anchoring and that the basic residues at positions 5 and 6 are especially important. We have demonstrated that C11orf83 depletion in HeLa cells induced a decrease in ATP level due to impaired respiration. Although the enzymatic activities of the five RC complexes were found to be affected by this depletion, C11orf83 was shown to be specifically required for the early stages of bc_1 complex assembly, probably by stabilizing the bc_1 core complex. We observed that C11orf83 loss also induced a clear decrease in the abundance of the III_2/IV and I/III_2/IV SC and a disorganization of the mitochondrial ultrastructure. These two observations are probably linked, since crista morphology maintenance and SC formation have been shown to be connected (60). These mitochondrial ultrastructure defects may also explain the reduced enzymatic activities of all the ETC complexes, as reported for OPA1-depleted cells (63). A recent study highlighted that OPA1 oligomerization was required both to modulate crista ultrastructure and to regulate complex V assembly by stabilizing the expression of the F_0 subunit MT-ATP6 (70). In C11orf83-deficient cells, OPA1-containing complexes were disturbed and complex V activity was decreased. Therefore, we can speculate that the lower complex V activity observed in the absence of C11orf83 may be due to a deficiency of the F_0 subunit of complex V. In addition, we demonstrated that C11orf83 depletion led to a higher sensitivity to actinomycin D-induced apoptosis. Since the remodelling of the cristae seems to be a prerequisite to apoptosis (71), we suspect that this may also be a consequence of the IM destabilization. Finally, since crista alteration and reduced RC activity were reported to occur in aged cells (42–46, 72), we suspect that mitochondrial dysfunctions observed in C11orf83-depleted cells could explain their growth deficit after several passages.

We have shown that the OMA1 metalloprotease mediates the cleavage of C11orf83 in response to mitochondrial depolarization. Given our results for C11orf83-depleted cells, we can hypothesize

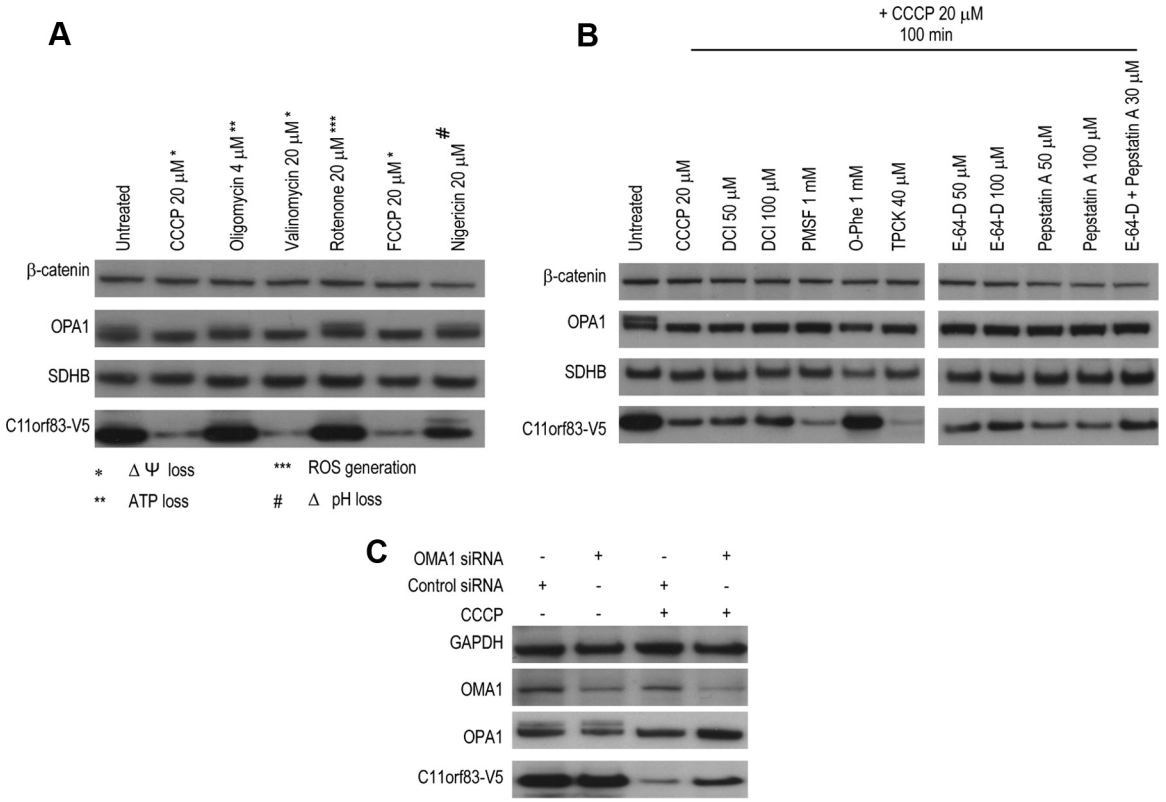

FIG 9 C11orf83, like OPA1, is cleaved by OMA1 under ΔΨ loss. (A) Analysis of the stress-induced proteolysis of C11orf83 compared to OPA1. HeLa cells expressing C11orf83-V5 were treated with mitochondrion-damaging agents for 3 h, and cell lysates were analyzed by immunoblotting after SDS-PAGE. β-Catenin and SDHB were used as loading controls for cytosolic and mitochondrial proteins. Stress-induced cleavage of OPA1 and C11orf83 was observed by antibodies against OPA1 and the V5 tag. ROS, reactive oxygen species. (B) Analysis of the sensitivity of CCCP-induced cleavage of C11orf83 to various protease inhibitors. HeLa cells expressing C11orf83-V5 were incubated with CCCP with or without protease inhibitors. Cells lysates were fractionated by SDS-PAGE and analyzed by immunoblotting. β-Catenin and SDHB were used as loading controls. The prevention of C11orf83-V5 proteolysis was monitored thanks to an antibody against the V5 tag. (C) OMA1 involvement in the stress-induced cleavage of C11orf83. HeLa cells were transfected with C11orf83-V5 and treated with control siRNA or siRNA against OMA1. Forty-eight hours after siRNA transfection, cells were incubated with or without CCCP and cell lysates were analyzed by immunoblotting, after SDS-PAGE, using antibodies against OMA1, OPA1, and the V5 tag. GAPDH was used as a loading control. The two bands detected by the antibody against OPA1 in the absence of CCCP correspond to short and long OPA1 isoforms. The degradation of endogenous C11orf83 under CCCP treatment (lane 3) was prevented by the depletion of OMA1 (lane 4).

that the specific proteolysis of C11orf83 by OMA1 in cells with depolarized mitochondria may destabilize the respiratory SC, inducing crista disorganization and increasing their sensitivity to apoptosis. To our knowledge, there is no other example of an assembly factor or a respiratory complex subunit which would be a target of OMA1 proteolysis upon stress. In contrast, it is well known that OPA1 is cleaved by OMA1 upon mitochondrial depolarization, like C11orf83, and that this induces mitochondrial fission and crista disorganization, resulting in enhanced apoptosis sensitivity (67, 68, 73).

During our study, we found a specific interaction of C11orf83 with the bc_1 complex. However, since we observed that C11orf83 comigrated not only with the bc_1 complex and III_2/IV SC in native gels but also with complex IV, we cannot exclude a transient interaction of C11orf83 with complex IV. A similar case has been recently described for *S. cerevisiae*: Rcf1p, identified both as an assembly factor for complex IV and as a stabilizing factor of the III_2/IV_2 SC (21), stably interacts with complex IV and also weakly binds to the bc_1 complex (74). Furthermore, since we did not detect C11orf83 in the I/III_2/IV SC, we propose that C11orf83 could be involved in the stabilization of the III_2/IV SC and be removed when this smaller SC associates with complex I. The formation of the I/III_2/IV SC could stabilize the interaction between complexes III_2 and IV, rendering C11orf83 stabilizing function redundant and leading to the elimination of this protein from the SC. In the literature, the complex I assembly chaperone mimitin (NDUFAF2) is also described as being transiently used for a specific step of assembly and then released to allow assembly completion (75).

Finally, we showed that C11orf83 was able to bind to CL and to its precursor PA (76). CL is an important IM phospholipid involved in the stabilization of individual ETC complexes and SC (49, 51, 52, 77). Several phospholipid-binding sites were described for the bc_1 complex and complex IV, among which some are specific to CL (56, 57, 78). For the bc_1 complex, most of these CL sites were identified on the matrix side of the IM bilayer or in the transmembrane domains of proteins like Cyt1p or Cytbp (59, 78). However, interactions of CL with ETC complexes on the IMS leaflet of the IM were previously reported for cytochrome *c* (79) and for complex IV (57) and might be involved in the formation and stabilization of the III_2/IV SC (57). Similarly, we propose that the CL-binding properties of the IMS-protruding C11orf83

would be involved in the stabilization of III_2/IV SC, which might explain the reduction of the abundance of III_2/IV SC observed after C11orf83 depletion. We found that the CL binding of C11orf83 did not require its N-terminal part, responsible for IM targeting and anchoring, but required both α-helices of the IMS part, indicating that they provide a unique tertiary structure suitable for the interaction with CL. Similar observations were reported for the truncated proapoptotic protein tBid, whose CL-binding domain encompasses three helices, H4, H5, and H6 (80). Studies on the composition of the CL binding sites of the RC complexes highlighted that the side chains of positively charged amino acids (lysine and arginine) were frequently involved in electrostatic bonds with CL due to CL's negative charge (57, 78, 81). Phenylalanine and leucine residues were also found to be involved in CL binding sites of complexes I and III (57). In addition, amino acids which contribute to CL binding are often well conserved over species (78). According to these data, we introduced several mutations in GST-C11orf83 (L24A, K35A, K40A, R55A, and R87A) and assessed the CL binding of these mutated forms. Unfortunately, none of these point mutations impaired the CL binding ability of C11orf83 (data not shown). Additional structural investigations by X-ray crystallography coupled to extensive site-directed mutagenesis studies would be needed to characterize the interaction of C11orf83 with CL at the molecular level.

We noticed that C11orf83-deficient cells presented some features similar to those observed following depletion of proteins involved in CL synthesis. HeLa cells downregulating the CL synthase showed an increased susceptibility to cell death due to an accumulation of free cytochrome *c* in the IMS of mitochondria with disorganized cristae (82). In these CL synthase-downregulating cells, the level of CL is still detectable and sufficient to sustain a normal OXPHOS. In contrast, lymphoblasts from patients with Barth syndrome (BTHS) (83), a genetic disease caused by mutations in the TAZ gene encoding tafazzin, an enzyme involved in CL maturation, showed severe mitochondrial respiratory deficiencies due to a destabilization of respiratory SC, reduced enzymatic activities of complexes I, III, and IV, and defects in mitochondrial ultrastructure (52, 84). In addition, tissues of BTHS patients and TAZ-deficient cells revealed accumulation of monolyso-CL (a remodeling intermediate) and an abnormal composition of CL showing a shift to less saturated acyl chains (85, 86). These changes in CL composition are thought to perturb the mitochondrial membrane and cause the disorganized cristae. Although we showed that the total amount of CL was not altered in C11orf83-deficient cells, we did observe a subtle but significant increase in CL species enriched in C_{16} fatty acids. The CL acyl chain composition in general is known to vary between organisms and between tissues and cell types within the same organism (87, 88). These differences are thought to have a structural role in membranes and/or allow adaptation against environmental stress (88). Therefore, the changes observed in CL fatty acid composition in the absence of C11orf83 could represent an adaptation of the cell to cope with disorganized cristae and an impaired OXPHOS.

In summary, we identified and characterized C11orf83 as a new factor required for the assembly of the bc_1 complex and for the stabilization of SC, which binds CL and is specifically cleaved by OMA1 upon stress. No obvious ortholog of C11orf83 was found by BLAST analysis in lower eukaryotes. However, a literature review indicated that *S. cerevisiae* Cbp4p, compared to C11orf83, has the same mitochondrial localization and topology, with an hydrophobic α-helix of around 20 aa (23 for C11orf83 and 22 for Cbp4p) at its N terminus involved in mitochondrial membrane targeting and anchoring (89) and a C-terminal part exposed in the IMS. In addition, C11orf83-deficient human cells and *cbp4*Δ mutant yeast strains display identical accumulations of CYC1/Cyt1p-containing subcomplexes and similarly reduced steady-state levels of UQCRB/Qcr7p and UQCRQ/Qcr8p, indicating that Cbp4p and C11orf83 have similar implications in the early stages of bc_1 complex assembly (90). Therefore, C11orf83 may be the functional homolog of Cbp4p in humans. During the writing of the manuscript, Wanschers and colleagues proposed that C11orf83, which they renamed UQCC3, would be the human ortholog of Cbp4p. They identified a missense mutation in C11orf83 (Val20Glu) that resulted in the destabilization of the protein in a patient and caused a bc_1 complex deficiency (91). In addition to these findings, we have demonstrated that C11orf83 interacts with the bc_1 complex. Although Kronekova and Rödel observed that Cbp4p-containing complexes comigrated with complex III_2 and weakly with the III_2/IV SC (90), no interaction between Cbp4p and either the bc_1 complex or complex IV had yet been reported. We also demonstrated that C11orf83 is involved in the SC stabilization and binds to CL, two important features which had never been studied in yeast. Importantly, Wanschers and colleagues reported that *cbp4*Δ mutant yeast strains could not be complemented by C11orf83 (91). This result could be due to a low level of sequence similarity between Cbp4p and C11orf83. For example, the RK motif, which we found to be essential for C11orf83 mitochondrial localization (Fig. 1A, E, and H), is present in higher eukaryotes but not in yeast. These variations of sequence may explain the not fully overlapping properties observed between Cbp4p and C11orf83, reflecting the mitochondrial ETC evolutionary differences between *S. cerevisiae* and Metazoa.

ACKNOWLEDGMENTS

We thank Denis Martinvalet, Oliver Hartley, Maureen Deehan, Paula Duek, Rachel Porcelli, Marianne Paolini-Bertrand, and Irène Rossitto-Borlat for comments and suggestions, review of the manuscript, and technical assistance, and we thank Mathias Uhlen (Human Protein Atlas, Sweden) for providing a number of rabbit polyclonal antibodies against mitochondrial proteins. We thank the PFMU at the Faculty of Medicine, Geneva, Switzerland, for access to transmission electron microscopy equipment and M. A. T. Vervaart, Laboratory Genetic Diseases, Amsterdam, The Netherlands, for performing the CL MS analysis.

This work was supported by the Faculty of Medicine of the University of Geneva, the Swiss National Science Foundation (grant no. 310030-152618 and CRSII3-141798 to M.F.), and the Ernst and Lucie Schmidheiny Foundation (grant to M.D.).

REFERENCES

1. **Ghezzi D, Zeviani M.** 2012. Assembly factors of human mitochondrial respiratory chain complexes: physiology and pathophysiology. Adv Exp Med Biol **748:**65–106. http://dx.doi.org/10.1007/978-1-4614-3573-0_4.
2. **Schägger H.** 2001. Respiratory chain supercomplexes. IUBMB Life **52:** 119–128. http://dx.doi.org/10.1080/15216540152845911.
3. **Iwata S, Lee JW, Okada K, Lee JK, Iwata M, Rasmussen B, Link TA, Ramaswamy S, Jap BK.** 1998. Complete structure of the 11-subunit bovine mitochondrial cytochrome bc_1 complex. Science **281:**64–71. http://dx.doi.org/10.1126/science.281.5373.64.
4. **Schägger H, Link TA, Engel WD, von Jagow G.** 1986. Isolation of the eleven protein subunits of the bc_1 complex from beef heart. Methods Enzymol **126:** 224–237. http://dx.doi.org/10.1016/S0076-6879(86)26024-3.

5. **Zara V, Conte L, Trumpower BL.** 2007. Identification and characterization of cytochrome bc(1) subcomplexes in mitochondria from yeast with single and double deletions of genes encoding cytochrome bc(1) subunits. FEBS J **274:**4526–4539. http://dx.doi.org/10.1111/j.1742-4658.2007.05982.x.
6. **Smith PM, Fox JL, Winge DR.** 2012. Biogenesis of the cytochrome bc(1) complex and role of assembly factors. Biochim Biophys Acta **1817:**276–286. http://dx.doi.org/10.1016/j.bbabio.2011.11.009.
7. **Lange C, Hunte C.** 2002. Crystal structure of the yeast cytochrome bc_1 complex with its bound substrate cytochrome c. Proc Natl Acad Sci U S A **99:**2800–2805. http://dx.doi.org/10.1073/pnas.052704699.
8. **Fernandez-Vizarra E, Bugiani M, Goffrini P, Carrara F, Farina L, Procopio E, Donati A, Uziel G, Ferrero I, Zeviani M.** 2007. Impaired complex III assembly associated with BCS1L gene mutations in isolated mitochondrial encephalopathy. Hum Mol Genet **16:**1241–1252. http://dx.doi.org/10.1093/hmg/ddm072.
9. **Ghezzi D, Arzuffi P, Zordan M, Da Re C, Lamperti C, Benna C, D'Adamo P, Diodato D, Costa R, Mariotti C, Uziel G, Smiderle C, Zeviani M.** 2011. Mutations in TTC19 cause mitochondrial complex III deficiency and neurological impairment in humans and flies. Nat Genet **43:**259–263. http://dx.doi.org/10.1038/ng.761.
10. **Tucker EJ, Wanschers BFJ, Szklarczyk R, Mountford HS, Wijeyeratne XW, van den Brand MAM, Leenders AM, Rodenburg RJ, Reljić B, Compton AG, Frazier AE, Bruno DL, Christodoulou J, Endo H, Ryan MT, Nijtmans LG, Huynen MA, Thorburn DR.** 2013. Mutations in the UQCC1-interacting protein, UQCC2, cause human complex III deficiency associated with perturbed cytochrome b protein expression. PLoS Genet **9:**e1004034. http://dx.doi.org/10.1371/journal.pgen.1004034.
11. **Sánchez E, Lobo T, Fox JL, Zeviani M, Winge DR, Fernández-Vizarra E.** 2013. LYRM7/MZM1L is a UQCRFS1 chaperone involved in the last steps of mitochondrial complex III assembly in human cells. Biochim Biophys Acta **1827:**285–293. http://dx.doi.org/10.1016/j.bbabio.2012.11.003.
12. **Kotarsky H, Karikoski R, Mörgelin M, Marjavaara S, Bergman P, Zhang D-L, Smet J, van Coster R, Fellman V.** 2010. Characterization of complex III deficiency and liver dysfunction in GRACILE syndrome caused by a BCS1L mutation. Mitochondrion **10:**497–509. http://dx.doi.org/10.1016/j.mito.2010.05.009.
13. **Acín-Pérez R, Fernández-Silva P, Peleato ML, Pérez-Martos A, Enriquez JA.** 2008. Respiratory active mitochondrial supercomplexes. Mol Cell **32:**529–539. http://dx.doi.org/10.1016/j.molcel.2008.10.021.
14. **Genova ML, Lenaz G.** 2014. Functional role of mitochondrial respiratory supercomplexes. Biochim Biophys Acta **1837:**427–443. http://dx.doi.org/10.1016/j.bbabio.2013.11.002.
15. **Maranzana E, Barbero G, Falasca AI, Lenaz G, Genova ML.** 2013. Mitochondrial respiratory supercomplex association limits production of reactive oxygen species from complex I. Antioxid Redox Signal **19:**1469–1480. http://dx.doi.org/10.1089/ars.2012.4845.
16. **Moreno-Lastres D, Fontanesi F, García-Consuegra I, Martín MA, Arenas J, Barrientos A, Ugalde C.** 2012. Mitochondrial complex I plays an essential role in human respirasome assembly. Cell Metab **15:**324–335. http://dx.doi.org/10.1016/j.cmet.2012.01.015.
17. **Lazarou M, Smith SM, Thorburn DR, Ryan MT, McKenzie M.** 2009. Assembly of nuclear DNA-encoded subunits into mitochondrial complex IV, and their preferential integration into supercomplex forms in patient mitochondria. FEBS J **276:**6701–6713. http://dx.doi.org/10.1111/j.1742-4658.2009.07384.x.
18. **Lapuente-Brun E, Moreno-Loshuertos R, Acín-Pérez R, Latorre-Pellicer A, Colás C, Balsa E, Perales-Clemente E, Quirós PM, Calvo E, Rodríguez-Hernández MA, Navas P, Cruz R, Carracedo ´A, López-Otín C, Pérez-Martos A, Fernández-Silva P, Fernández-Vizarra E, Enríquez JA.** 2013. Supercomplex assembly determines electron flux in the mitochondrial electron transport chain. Science **340:**1567–1570. http://dx.doi.org/10.1126/science.1230381.
19. **Ikeda K, Shiba S, Horie-Inoue K, Shimokata K, Inoue S.** 2013. A stabilizing factor for mitochondrial respiratory supercomplex assembly regulates energy metabolism in muscle. Nat Commun **4:**2147. http://dx.doi.org/10.1038/ncomms3147.
20. **Strogolova V, Furness A, Robb-McGrath M, Garlich J, Stuart RA.** 2012. Rcf1 and Rcf2, members of the hypoxia-induced gene 1 protein family, are critical components of the mitochondrial cytochrome bc_1-cytochrome *c* oxidase supercomplex. Mol Cell Biol **32:**1363–1373. http://dx.doi.org/10.1128/MCB.06369-11.
21. **Vukotic M, Oeljeklaus S, Wiese S, Vögtle FN, Meisinger C, Meyer HE, Zieseniss A, Katschinski DM, Jans DC, Jakobs S, Warscheid B, Rehling P, Deckers M.** 2012. Rcf1 mediates cytochrome oxidase assembly and respirasome formation, revealing heterogeneity of the enzyme complex. Cell Metab **15:**336–347. http://dx.doi.org/10.1016/j.cmet.2012.01.016.
22. **Taylor SW, Fahy E, Ghosh SS.** 2003. Global organellar proteomics. Trends Biotechnol **21:**82–88. http://dx.doi.org/10.1016/S0167-7799(02)00037-9.
23. **Taylor SW, Fahy E, Zhang B, Glenn GM, Warnock DE, Wiley S, Murphy AN, Gaucher SP, Capaldi RA, Gibson BW, Ghosh SS.** 2003. Characterization of the human heart mitochondrial proteome. Nat Biotechnol **21:**281–286. http://dx.doi.org/10.1038/nbt793.
24. **Pagliarini DJ, Calvo SE, Chang B, Sheth SA, Vafai SB, Ong S-E, Walford GA, Sugiana C, Boneh A, Chen WK, Hill DE, Vidal M, Evans JG, Thorburn DR, Carr SA, Mootha VK.** 2008. A mitochondrial protein compendium elucidates complex I disease biology. Cell **134:**112–123. http://dx.doi.org/10.1016/j.cell.2008.06.016.
25. **Cotter D, Guda P, Fahy E, Subramaniam S.** 2004. MitoProteome: mitochondrial protein sequence database and annotation system. Nucleic Acids Res **32:**D463–D467. http://dx.doi.org/10.1093/nar/gkh048.
26. **Uhlen M, Oksvold P, Fagerberg L, Lundberg E, Jonasson K, Forsberg M, Zwahlen M, Kampf C, Wester K, Hober S, Wernerus H, Björling L, Ponten F.** 2010. Towards a knowledge-based Human Protein Atlas. Nat Biotechnol **28:**1248–1250. http://dx.doi.org/10.1038/nbt1210-1248.
27. **Mary C, Duek P, Salleron L, Tienz P, Bumann D, Bairoch A, Lane L.** 2012. Functional identification of APIP as human mtnB, a key enzyme in the methionine salvage pathway. PLoS One **7:**e52877. http://dx.doi.org/10.1371/journal.pone.0052877.
28. **Spinazzi M, Casarin A, Pertegato V, Salviati L, Angelini C.** 2012. Assessment of mitochondrial respiratory chain enzymatic activities on tissues and cultured cells. Nat Protoc **7:**1235–1246. http://dx.doi.org/10.1038/nprot.2012.058.
29. **Kramarova TV, Shabalina IG, Andersson U, Westerberg R, Carlberg I, Houstek J, Nedergaard J, Cannon B.** 2008. Mitochondrial ATP synthase levels in brown adipose tissue are governed by the c-Fo subunit P1 isoform. FASEB J **22:**55–63.
30. **Bligh EG, Dyer WJ.** 1959. A rapid method of total lipid extraction and purification. Can J Biochem Physiol **37:**911–917. http://dx.doi.org/10.1139/o59-099.
31. **Rouser G, Fkeischer S, Yamamoto A.** 1970. Two dimensional thin layer chromatographic separation of polar lipids and determination of phospholipids by phosphorus analysis of spots. Lipids **5:**494–496. http://dx.doi.org/10.1007/BF02531316.
32. **Houtkooper RH, Rodenburg RJ, Thiels C, van Lenthe H, Stet F, Poll-The BT, Stone JE, Steward CG, Wanders RJ, Smeitink J, Kulik W, Vaz FM.** 2009. Cardiolipin and monolysocardiolipin analysis in fibroblasts, lymphocytes, and tissues using high-performance liquid chromatography-mass spectrometry as a diagnostic test for Barth syndrome. Anal Biochem **387:**230–237. http://dx.doi.org/10.1016/j.ab.2009.01.032.
33. **Foti M, Carpentier JL, Aiken C, Trono D, Lew DP, Krause KH.** 1997. Second-messenger regulation of receptor association with clathrin-coated pits: a novel and selective mechanism in the control of CD4 endocytosis. Mol Biol Cell **8:**1377–1389. http://dx.doi.org/10.1091/mbc.8.7.1377.
34. **Notredame C, Higgins DG, Heringa J.** 2000. T-Coffee: a novel method for fast and accurate multiple sequence alignment. J Mol Biol **302:**205–217. http://dx.doi.org/10.1006/jmbi.2000.4042.
35. **Jones DT.** 1999. Protein secondary structure prediction based on position-specific scoring matrices. J Mol Biol **292:**195–202. http://dx.doi.org/10.1006/jmbi.1999.3091.
36. **Bond CS, Schüttelkopf AW.** 2009. ALINE: a WYSIWYG protein-sequence alignment editor for publication-quality alignments. Acta Crystallogr D Biol Crystallogr **65:**510–512. http://dx.doi.org/10.1107/S0907444909007835.
37. **Hunter S, Jones P, Mitchell A, Apweiler R, Attwood TK, Bateman A, Bernard T, Binns D, Bork P, Burge S, de Castro E, Coggill P, Corbett M, Das U, Daugherty L, Duquenne L, Finn RD, Fraser M, Gough J, Haft D, Hulo N, Kahn D, Kelly E, Letunic I, Lonsdale D, Lopez R, Madera M, Maslen J, McAnulla C, McDowall J, McMenamin C, Mi H, Mutowo-Muellenet P, Mulder N, Natale D, Orengo C, Pesseat S, Punta M, Quinn AF, Rivoire C, Sangrador-Vegas A, Selengut JD, Sigrist CJA, Scheremetjew M, Tate J, Thimmajanarthanan M, Thomas PD, Wu CH, Yeats C, Yong S-Y, Lees J, Perkins J, Sillitoe I, Rentzsch R, Dessailly BH.** 2012. InterPro in 2011: new developments in the family and domain prediction database. Nucleic Acids Res **40:**4725. http://dx.doi.org/10.1093/nar/gks456.

38. **Söding J, Biegert A, Lupas AN.** 2005. The HHpred interactive server for protein homology detection and structure prediction. Nucleic Acids Res **33:**W244–W248. http://dx.doi.org/10.1093/nar/gki408.
39. **Clark HF, Gurney AL, Abaya E, Baker K, Baldwin D, Brush J, Chen J, Chow B, Chui C, Crowley C, Currell B, Deuel B, Dowd P, Eaton D, Foster J, Grimaldi C, Gu Q, Hass PE, Heldens S, Huang A, Kim HS, Klimowski L, Jin Y, Johnson S, Lee J, Lewis L, Liao D, Mark M, Robbie E, Sanchez C, Schoenfeld J, Seshagiri S, Simmons L, Singh J, Smith V, Stinson J, Vagts A, Vandlen R, Watanabe C, Wieand D, Woods K, Xie M-H, Yansura D, Yi S, Yu G, Yuan J, Zhang M, Zhang Z, Goddard A, Wood WI, Godowski P, Gray A.** 2003. The secreted protein discovery initiative (SPDI), a large-scale effort to identify novel human secreted and transmembrane proteins: a bioinformatics assessment. Genome Res **13:** 2265–2270. http://dx.doi.org/10.1101/gr.1293003.
40. **Zhang Z, Henzel WJ.** 2004. Signal peptide prediction based on analysis of experimentally verified cleavage sites. Protein Sci **13:**2819–2824. http://dx.doi.org/10.1110/ps.04682504.
41. **Catherman AD, Li M, Tran JC, Durbin KR, Compton PD, Early BP, Thomas PM, Kelleher NL.** 2013. Top down proteomics of human membrane proteins from enriched mitochondrial fractions. Anal Chem **85:** 1880–1888. http://dx.doi.org/10.1021/ac3031527.
42. **Bratic A, Larsson N-G.** 2013. The role of mitochondria in aging. J Clin Invest **123:**951–957. http://dx.doi.org/10.1172/JCI64125.
43. **Shigenaga MK, Hagen TM, Ames BN.** 1994. Oxidative damage and mitochondrial decay in aging. Proc Natl Acad Sci U S A **91:**10771–10778. http://dx.doi.org/10.1073/pnas.91.23.10771.
44. **Yen TC, Chen YS, King KL, Yeh SH, Wei YH.** 1989. Liver mitochondrial respiratory functions decline with age. Biochem Biophys Res Commun **165:**944–1003.
45. **Short KR, Bigelow ML, Kahl J, Singh R, Coenen-Schimke J, Raghavakaimal S, Nair KS.** 2005. Decline in skeletal muscle mitochondrial function with aging in humans. Proc Natl Acad Sci U S A **102:**5618–5623. http://dx.doi.org/10.1073/pnas.0501559102.
46. **Stocco DM, Cascarano J, Wilson MA.** 1977. Quantitation of mitochondrial DNA, RNA, and protein in starved and starved-refed rat liver. J Cell Physiol **90:**295–306. http://dx.doi.org/10.1002/jcp.1040900215.
47. **American Type Culture Collection.** 2003. Reference strains: how many passages are too many? ATCC Connect **23:**6–7.
48. **Schägger H, Pfeiffer K.** 2001. The ratio of oxidative phosphorylation complexes I–V in bovine heart mitochondria and the composition of respiratory chain supercomplexes. J Biol Chem **276:**37861–37867. http://dx.doi.org/10.1074/jbc.M106474200.
49. **Wenz T, Hielscher R, Hellwig P, Schägger H, Richers S, Hunte C.** 2009. Role of phospholipids in respiratory cytochrome bc(1) complex catalysis and supercomplex formation. Biochim Biophys Acta **1787:**609–616. http://dx.doi.org/10.1016/j.bbabio.2009.02.012.
50. **Bazán S, Mileykovskaya E, Mallampalli VKPS, Heacock P, Sparagna GC, Dowhan W.** 2013. Cardiolipin-dependent reconstitution of respiratory supercomplexes from purified Saccharomyces cerevisiae complexes III and IV. J Biol Chem **288:**401–411. http://dx.doi.org/10.1074/jbc.M112.425876.
51. **Althoff T, Mills DJ, Popot J-L, Kühlbrandt W.** 2011. Arrangement of electron transport chain components in bovine mitochondrial supercomplex I1III2IV1. EMBO J **30:**4652–4664. http://dx.doi.org/10.1038/emboj.2011.324.
52. **McKenzie M, Lazarou M, Thorburn DR, Ryan MT.** 2006. Mitochondrial respiratory chain supercomplexes are destabilized in Barth syndrome patients. J Mol Biol **361:**462–469. http://dx.doi.org/10.1016/j.jmb.2006.06.057.
53. **Dowler S, Kular G, Alessi DR.** 2002. Protein lipid overlay assay. Sci STKE **2002:**pl6. http://dx.doi.org/10.1126/stke.2002.129.pl6.
54. **Xiao S, Finkielstein CV, Capelluto DGS.** 2013. The enigmatic role of sulfatides: new insights into cellular functions and mechanisms of protein recognition. Adv Exp Med Biol **991:**27–40. http://dx.doi.org/10.1007/978-94-007-6331-9_3.
55. **Chakraborty TR.** 1999. Phosphatidic acid synthesis in mitochondria. Topography of formation and transmembrane migration. J Biol Chem **274:** 29786–29790.
56. **Palsdottir H, Hunte C.** 2004. Lipids in membrane protein structures. Biochim Biophys Acta **1666:**2–18. http://dx.doi.org/10.1016/j.bbamem.2004.06.012.
57. **Arnarez C, Marrink SJ, Periole X.** 2013. Identification of cardiolipin binding sites on cytochrome c oxidase at the entrance of proton channels. Sci Rep **3:**1263. http://dx.doi.org/10.1038/srep01263.
58. **Liu J, Durrant D, Yang H-S, He Y, Whitby FG, Myszka DG, Lee RM.** 2005. The interaction between tBid and cardiolipin or monolysocardiolipin. Biochem Biophys Res Commun **330:**865–870. http://dx.doi.org/10.1016/j.bbrc.2005.03.048.
59. **Lange C, Nett JH, Trumpower BL, Hunte C.** 2001. Specific roles of protein-phospholipid interactions in the yeast cytochrome bc_1 complex structure. EMBO J **20:**6591–6600. http://dx.doi.org/10.1093/emboj/20.23.6591.
60. **Cogliati S, Frezza C, Soriano ME, Varanita T, Quintana-Cabrera R, Corrado M, Cipolat S, Costa V, Casarin A, Gomes LC, Perales-Clemente E, Salviati L, Fernandez-Silva P, Enriquez JA, Scorrano L.** 2013. Mitochondrial cristae shape determines respiratory chain supercomplexes assembly and respiratory efficiency. Cell **155:**160–171. http://dx.doi.org/10.1016/j.cell.2013.08.032.
61. **Olichon A, Emorine LJ, Descoins E, Pelloquin L, Brichese L, Gas N, Guillou E, Delettre C, Valette A, Hamel CP, Ducommun B, Lenaers G, Belenguer P.** 2002. The human dynamin-related protein OPA1 is anchored to the mitochondrial inner membrane facing the inter-membrane space. FEBS Lett **523:**171–176. http://dx.doi.org/10.1016/S0014-5793(02)02985-X.
62. **Olichon A, Baricault L, Gas N, Guillou E, Valette A, Belenguer P, Lenaers G.** 2003. Loss of OPA1 perturbates the mitochondrial inner membrane structure and integrity, leading to cytochrome c release and apoptosis. J Biol Chem **278:**7743–7746. http://dx.doi.org/10.1074/jbc.C200677200.
63. **Kushnareva YE, Gerencser AA, Bossy B, Ju W-K, White AD, Waggoner J, Ellisman MH, Perkins G, Bossy-Wetzel E.** 2013. Loss of OPA1 disturbs cellular calcium homeostasis and sensitizes for excitotoxicity. Cell Death Differ **20:**353–365. http://dx.doi.org/10.1038/cdd.2012.128.
64. **Frezza C, Cipolat S, Martins de Brito O, Micaroni M, Beznoussenko GV, Rudka T, Bartoli D, Polishuck RS, Danial NN, De Strooper B, Scorrano L.** 2006. OPA1 controls apoptotic cristae remodeling independently from mitochondrial fusion. Cell **126:**177–189. http://dx.doi.org/10.1016/j.cell.2006.06.025.
65. **Griparic L, Kanazawa T, van der Bliek AM.** 2007. Regulation of the mitochondrial dynamin-like protein Opa1 by proteolytic cleavage. J Cell Biol **178:**757–764. http://dx.doi.org/10.1083/jcb.200704112.
66. **Cipolat S, Rudka T, Hartmann D, Costa V, Serneels L, Craessaerts K, Metzger K, Frezza C, Annaert W, D'Adamio L, Derks C, Dejaegere T, Pellegrini L, D'Hooge R, Scorrano L, De Strooper B.** 2006. Mitochondrial rhomboid PARL regulates cytochrome c release during apoptosis via OPA1-dependent cristae remodeling. Cell **126:**163–175. http://dx.doi.org/10.1016/j.cell.2006.06.021.
67. **Head B, Griparic L, Amiri M, Gandre-Babbe S, van der Bliek AM.** 2009. Inducible proteolytic inactivation of OPA1 mediated by the OMA1 protease in mammalian cells. J Cell Biol **187:**959–966. http://dx.doi.org/10.1083/jcb.200906083.
68. **Ehses S, Raschke I, Mancuso G, Bernacchia A, Geimer S, Tondera D, Martinou J-C, Westermann B, Rugarli EI, Langer T.** 2009. Regulation of OPA1 processing and mitochondrial fusion by m-AAA protease isoenzymes and OMA1. J Cell Biol **187:**1023–1036. http://dx.doi.org/10.1083/jcb.200906084.
69. **Chan NC, Salazar AM, Pham AH, Sweredoski MJ, Kolawa NJ, Graham RLJ, Hess S, Chan DC.** 2011. Broad activation of the ubiquitin-proteasome system by Parkin is critical for mitophagy. Hum Mol Genet **20:**1726–1737. http://dx.doi.org/10.1093/hmg/ddr048.
70. **Patten DA, Wong J, Khacho M, Soubannier V, Mailloux RJ, Pilon-Larose K, MacLaurin JG, Park DS, McBride HM, Trinkle-Mulcahy L, Harper M-E, Germain M, Slack RS.** 2014. OPA1-dependent cristae modulation is essential for cellular adaptation to metabolic demand. EMBO J **33:**2676–2691. http://dx.doi.org/10.15252/embj.201488349.
71. **Heath-Engel HM, Shore GC.** 2006. Mitochondrial membrane dynamics, cristae remodelling and apoptosis. Biochim Biophys Acta **1763:**549–560. http://dx.doi.org/10.1016/j.bbamcr.2006.02.006.
72. **Miquel J, Economos AC, Fleming J, Johnson JE.** 1980. Mitochondrial role in cell aging. Exp Gerontol **15:**575–591. http://dx.doi.org/10.1016/0531-5565(80)90010-8.
73. **Anand R, Wai T, Baker MJ, Kladt N, Schauss AC, Rugarli E, Langer T.** 2014. The i-AAA protease YME1L and OMA1 cleave OPA1 to balance mitochondrial fusion and fission. J Cell Biol **204:**919–929. http://dx.doi.org/10.1083/jcb.201308006.
74. **Chen Y-C, Taylor EB, Dephoure N, Heo J-M, Tonhato A, Papandreou**

I, Nath N, Denko NC, Gygi SP, Rutter J. 2012. Identification of a protein mediating respiratory supercomplex stability. Cell Metab **15:**348–360. http://dx.doi.org/10.1016/j.cmet.2012.02.006.
75. **Lazarou M, McKenzie M, Ohtake A, Thorburn DR, Ryan MT.** 2007. Analysis of the assembly profiles for mitochondrial- and nuclear-DNA-encoded subunits into complex I. Mol Cell Biol **27:**4228–4237. http://dx.doi.org/10.1128/MCB.00074-07.
76. **Schlame M, Haldar D.** 1993. Cardiolipin is synthesized on the matrix side of the inner membrane in rat liver mitochondria. J Biol Chem **268:**74–79.
77. **Pfeiffer K, Gohil V, Stuart RA, Hunte C, Brandt U, Greenberg ML, Schägger H.** 2003. Cardiolipin stabilizes respiratory chain supercomplexes. J Biol Chem **278:**52873–52880. http://dx.doi.org/10.1074/jbc.M308366200.
78. **Arnarez C, Mazat J-P, Elezgaray J, Marrink S-J, Periole X.** 2013. Evidence for cardiolipin binding sites on the membrane-exposed surface of the cytochrome bc_1. J Am Chem Soc **135:**3112–3120. http://dx.doi.org/10.1021/ja310577u.
79. **Kagan VE, Bayir HA, Belikova NA, Kapralov O, Tyurina YY, Tyurin VA, Jiang J, Stoyanovsky DA, Wipf P, Kochanek PM, Greenberger JS, Pitt B, Shvedova AA, Borisenko G.** 2009. Cytochrome c/cardiolipin relations in mitochondria: a kiss of death. Free Radic Biol Med **46:**1439–1453. http://dx.doi.org/10.1016/j.freeradbiomed.2009.03.004.
80. **Lutter M, Fang M, Luo X, Nishijima M, Xie X, Wang X.** 2000. Cardiolipin provides specificity for targeting of tBid to mitochondria. Nat Cell Biol **2:**754–761. http://dx.doi.org/10.1038/35036395.
81. **Pöyry S, Cramariuc O, Postila PA, Kaszuba K, Sarewicz M, Osyczka A, Vattulainen I, Róg T.** 2013. Atomistic simulations indicate cardiolipin to have an integral role in the structure of the cytochrome bc_1 complex. Biochim Biophys Acta **1827:**769–778. http://dx.doi.org/10.1016/j.bbabio.2013.03.005.
82. **Choi S-Y, Gonzalvez F, Jenkins GM, Slomianny C, Chretien D, Arnoult D, Petit PX, Frohman MA.** 2007. Cardiolipin deficiency releases cytochrome c from the inner mitochondrial membrane and accelerates stimuli-elicited apoptosis. Cell Death Differ **14:**597–606. http://dx.doi.org/10.1038/sj.cdd.4402020.
83. **Schlame M, Ren M.** 2006. Barth syndrome, a human disorder of cardiolipin metabolism. FEBS Lett **580:**5450–5455. http://dx.doi.org/10.1016/j.febslet.2006.07.022.
84. **Acehan D, Xu Y, Stokes DL, Schlame M.** 2007. Comparison of lymphoblast mitochondria from normal subjects and patients with Barth syndrome using electron microscopic tomography. Lab Invest **87:**40–48. http://dx.doi.org/10.1038/labinvest.3700480.
85. **Schlame M, Kelley RI, Feigenbaum A, Towbin JA, Heerdt PM, Schieble T, Wanders RJA, DiMauro S, Blanck TJJ.** 2003. Phospholipid abnormalities in children with Barth syndrome. J Am Coll Cardiol **42:**1994–1999. http://dx.doi.org/10.1016/j.jacc.2003.06.015.
86. **Richter-Dennerlein R, Korwitz A, Haag M, Tatsuta T, Dargazanli S, Baker M, Decker T, Lamkemeyer T, Rugarli EI, Langer T.** 2014. DNAJC19, a mitochondrial cochaperone associated with cardiomyopathy, forms a complex with prohibitins to regulate cardiolipin remodeling. Cell Metab **20:**158–171. http://dx.doi.org/10.1016/j.cmet.2014.04.016.
87. **Hoch FL.** 1992. Cardiolipins and biomembrane function. Biochim Biophys Acta **1113:**71–133. http://dx.doi.org/10.1016/0304-4157(92)90035-9.
88. **Schlame M, Ren M, Xu Y, Greenberg ML, Haller I.** 2005. Molecular symmetry in mitochondrial cardiolipins. Chem Phys Lipids **138:**38–49. http://dx.doi.org/10.1016/j.chemphyslip.2005.08.002.
89. **Crivellone MD.** 1994. Characterization of CBP4, a new gene essential for the expression of ubiquinol-cytochrome c reductase in Saccharomyces cerevisiae. J Biol Chem **269:**21284–21292.
90. **Kronekova Z, Rödel G.** 2005. Organization of assembly factors Cbp3p and Cbp4p and their effect on bc(1) complex assembly in Saccharomyces cerevisiae. Curr Genet **47:**203–212. http://dx.doi.org/10.1007/s00294-005-0561-9.
91. **Wanschers BFJ, Szklarczyk R, van den Brand MAM, Jonckheere A, Suijskens J, Smeets R, Rodenburg RJ, Stephan K, Helland IB, Elkamil A, Rootwelt T, Ott M, van den Heuvel L, Nijtmans LG, Huynen MA.** 2014. A mutation in the human CBP4 ortholog UQCC3 impairs complex III assembly, activity and cytochrome b stability. Hum Mol Genet **23:**6356–6365. http://dx.doi.org/10.1093/hmg/ddu357.